Physics Reports 537 (2014) 123–156

Contents lists available at ScienceDirect

Physics Reports

journal homepage: www.elsevier.com/locate/physrep

Excited states structure and processes: Understanding organic light-emitting diodes at the molecular level

Zhigang Shuai [a,*], Qian Peng [b]

[a] MOE Key Laboratory of Organic OptoElectronics and Molecular Engineering, Department of Chemistry, Tsinghua University, 100084 Beijing, PR China

[b] Beijing National Laboratory for Molecular Science (BNLMS), Institute of Chemistry, Chinese Academy of Sciences, 100190 Beijing, PR China

ARTICLE INFO

Article history:
Accepted 4 December 2013
Available online 14 December 2013
editor: S. Peyerimhoff

ABSTRACT

Photo- or electro-excited states in polyatomic molecules, aggregates, and conjugated polymers are at the center of organic light-emitting diodes (OLEDs). These can decay radiatively or non-radiatively, determining the luminescence quantum efficiency of molecular materials. According to Kasha's rule, light-emission is dictated by the lowest-lying excited state. For conjugated polymers, the electron correlation effect can lead the lowest-lying excited state to the even-parity $2A_g$ state which is non-emissive. To understand the nature of the low-lying excited state structure, we developed the density matrix renormalization group (DMRG) theory and its symmetrization scheme for quantum chemistry applied to calculate the excited states structure. We found there are three types of $1B_u/2A_g$ crossover behaviors: with electron correlation strength U, with bond length alternation, and with conjugation length. These directly influence the light-emitting property.

For the electro-excitation, carriers (electron and hole) are injected independently, forming both singlet and triplet excited bound states with statistically 25% and 75% portions, respectively. We found that the exciton formation rate can depend on spin manifold, and for conjugated polymers, the singlet exciton can have larger formation rate leading to the internal electroluminescence quantum efficiency larger than the 25% spin statistical limit. It is originated from the interchain electron correlation as well as intrachain lattice relaxation.

For the dipole allowed emissive state, the radiative decay process via either spontaneous emission or stimulated emission can be computed from electronic structure plus vibronic couplings. The challenging issue lies in the non-radiative decay via non-adiabatic coupling and/or spin–orbit coupling. We developed a unified correlation function formalism for the excited state radiative and non-radiative decay rates. We emphasized the low-frequency mode mixing (Duschinsky rotation) effect on the non-radiative decay. We further combined the non-adiabatic coupling and spin–orbit coupling for the triplet state decay (phosphorescence) quantum efficiency. All the formalisms have been developed analytically, which have been applied to optical spectroscopy, aggregation-induced emission phenomena, and polymer photovoltaic property.

Contents

* Corresponding author. Tel.: +86 1062797689.
E-mail addresses: zgshuai@tsinghua.edu.cn, zgshuai@iccas.ac.cn (Z. Shuai), qpeng@iccas.ac.cn (Q. Peng).

0370-1573/$ – see front matter © 2013 Elsevier B.V. All rights reserved.
http://dx.doi.org/10.1016/j.physrep.2013.12.002

1. Introduction

The discovery of organic and polymeric light-emitting diodes (OLEDs) by Tang et al. [1] and Friend et al. [2] has opened the door of organic electronics, which now becomes a sizable industry. Conjugated organic materials or organic semiconductors have attracted tremendous attentions since then. In addition to OLEDs, there have been also remarkable progresses achieved for organic field-effect transistors [3], organic solar cells [4], bio- and chemico-sensors [5], organic spintronic devices [6] and molecular magnets [7] based on organic semiconductors. The electronic processes govern the optoelectronic properties. Especially, the structure and dynamics of the electronic excited state dictate light-emitting process. In a typical light-emitting diode, the organic semiconductors (OS), being organic molecules or conjugated polymers as prepared either by sublimation or by spin-casting, are sandwiched between two electrodes with different workfunctions. The anode consists of usually transparent conducting glass Indium-Tin-Oxide (ITO) with workfunction $\sim$5 eV and the cathode can be aluminum or calcium with lower workfunction. When a small voltage is applied to the device, electron is injected through the cathode and the hole through the anode into the OS. The free carriers migrate in the OS and meet to form bound state, the exciton, the linear combination of molecular excited states. For organic film, the exciton is usually of Frenkel type, namely, intermolecular charge transfer component is negligible in many cases. And in conjugated polymers, the exciton is eventually formed in a single chain with a size typically extended to a few unit cells [8].

According to Kasha's rule, the fluorescence is determined by the lowest electronic excited state [9]. Suppose the lowest molecular or polymeric excited state is dipole forbidden (by symmetry/parity reason for instance), there is no fluorescence. For example, polyacetylene in the neutral form is non-emissive, because of the long known fact that the lowest excited state in polyene is of even parity $2A_g$ state [10]. Earlier quantum chemistry calculation at the configuration interaction (CI) level found that though the single transition from the highest occupied molecular orbital (HOMO) to the lowest unoccupied molecular orbital (LUMO) is dipole-allowed, the dipole forbidden double excitation is stabilized by inclusion of electron correlation effect [11]. This is not only an important manifestation of electron correlation effect in conjugated polymers, but also serves as a border line for emissive and non-emissive polymers. Polyacetylene (PA), polydiacetylene (PDA), polythiophene (PT) etc. are non-emissive or weakly emissive, because their lowest excited state is of $2A_g$ type. Polyparaphenylene (PPP), polyparaphenylene vinylene (PPV), polyfluorene (PF) *etc.* are emissive due to the lowest excited state of $1B_u$ character. Soos et al. demonstrated that a single parameter, the bond-length alternation (δ), can serve as a structure indicator to distinguish them. Namely, for small δ the $2A_g$ state is below $1B_u$ [12]. It was found that the ordering of these two states is very sensitive to the level of theory treating electron correlation effect. Even for short polyene molecule, a CI with single excitation determinant always produces $2A_g > 1B_u$, while by inclusion of double and higher excitation determinants, one obtains just the opposite. This immediately calls for a reliable methodology for the low-lying excited state structure with proper treatment of electron correlation. CI based methods even at the multi-reference determinant (MRDCI) level suffer from both size-consistency and computational cost problems. But such calculations have indeed played important role in revealing the general picture, for example, by Tavan and Schulten [13]. Along the same line, Soos and collaborators had developed an extensive generalized valence bond (GVB) approach to investigate the photophysics of linear chain, which is exact solution for the model Hamiltonian [14]. The maximum size they can treat is 16–18 orbitals or electrons [15]. Due to the electron correlation difficulty, in practice, for a new polymer structure, theory nowadays cannot predict its light-emitting nature, even not qualitatively. As shown by Shuai and Brédas, the equation of motion method based on coupled cluster single and double excitation (EOM/CCSD) also failed to predict right ordering for larger than

22 π-orbitals of a linear polyene [16]. Modern computational chemistry has been largely developed based on density functional theory (DFT) and its excited state development of time-dependent density functional theory (TDDFT) [17]. Undoubtedly, DFT based methodology has completely changed the computational chemistry land scape. The standard and commonly practiced TDDFT (for instance based on B3LYP functional) does not allow a correct description for the excited state ordering. Recent developments in TDDFT by including double excitation character have been shown to be promising in reproducing the correct ordering for small molecules [18].

The approach we developed to look at the excited state ordering was along the line of "nearly exact" solution to model system, from Hubbard model ($t-U$ only) [19] to the extended Hubbard–Peierls (t, δ, U, V) model, and to the semiempirical quantum chemistry Pariser–Parr–Pople (long-range Coulomb potential) model [20]. These models capture the essential electron-correlation effect in conjugated polymer. Following the original idea of density matrix renormalization group (DMRG) proposed by White in 1992 [21], we have made the following developments: (i) introduction of a symmetrization scheme in 1996 by Ramasesha et al. which divides the renormalized Hilbert space according to spatial inversion, spin-flip, and charge conjugation symmetry [22]. This not only reduces the computational costs, but most importantly allows facile excited state targeting by excluding the intruding spaces; (ii) extension in 1997 to the long-range potential so that a general quantum chemistry model can be dealt with for very high precision [23]; (iii) introduction of linear and nonlinear response formalism in 1998 [24]. In this Report, we will introduce the work on the excited state ordering study from the DMRG consideration in Section 2 for understanding the polymer light-emitting property. Based on our understanding from correlated electrons, we also proposed a practical rule deriving from molecular orbital calculations to design light-emitting polymers with proper excited state ordering.

Prior to exciton formation in electroluminescence, charges carriers (electrons and holes) are injected into organic materials. The exciton can diffuse and decay radiatively or non-radiatively. Only the radiative decay gives rise to photon. The generated photo should escape the device through the ITO electrode, with most photons are reabsorbed within the device. The overall external quantum efficiency can be written as: $\eta = \eta_{rec}\eta_S\eta_{pl}\eta_{OC}$ [25]. These are ratios of exciton recombination from free carriers, portion of singlet exciton, photoluminescence efficiency, and the optical outcoupling constant (portion of photons which are not reabsorbed inside the device), respectively. The η_{OC} for organic device is generally believed to be about 0.2, or, only 20% of the generated photons can escape the device. Suppose all the carriers can form bound pair ($\eta_{rec} = 1$) and the photoluminescence quantum efficiency is 100%. Statistically, 1/4 will form singlet pairs and 3/4 triplet pairs, thus it is expected that singlet exciton formation portion is 25%. Then the overall external electroluminescence quantum efficiency is limited to 5% for fluorescence materials. One way to break this limit is to introduce heavy elements to enhance spin–orbit coupling [26,27]. If both singlet and triplet excited state can decay radiatively, the internal quantum efficiency can go up to 100%, as was demonstrated by Adachi et al. [28]. However, such picture has been challenged by Cao et al. experimentally [29] and by Shuai et al. theoretically [30]. These authors believed that indeed the 25% limit holds for small molecules, but for long conjugated chains, the exciton formation rate for singlet state can be larger than that of triplet state. Dynamically, the eventually formed singlet exciton portion is larger than 1/4. There have been immediate supports from ample spectroscopy evidences that singlet exciton formation rate is larger than the triplet state. Recent advances in spin dynamics in organic systems become even more important, including the magnetoresistance [31], magnetoelectroluminescence [32], spin-valves etc. [33]. Novel phenomena have been discovered with excitements. This is still an open area with mysteries. We will present our theoretical views on the spin-dependent exciton formation in Section 3.

Now, suppose a singlet or triplet excited state is formed. The next question is how it will decay. Namely, what are the radiative and non-radiative rates? The radiative decay is through the spontaneous emission which gives rise to photon. The electric dipole transition moment between the excited state and the ground state is the fundamental physical parameter. If this quantity is zero (for instance, for $2A_g$ state), light-emission is not allowed. This is fully understood and the transition rate can be easily computed through oscillator strength by virtue of Einstein's spontaneous radiation theory as $k_r \sim fE_g^2/1.5$ where f is the dimensionless oscillator strength and E_g is the transition gap (in unit of cm^{-1}) to give rise the rate in unit of s^{-1}. This becomes very complicated for polyatomic molecules with vibronic couplings. Apart from the difficulty for excited state geometry optimization and vibrational modes, the computational costs for Franck–Condon factors at finite temperature or the spectral density become intractable in the sum-over-vibrational-states formalism, especially, when Duschinsky rotation and/or Herzberg–Teller effects are taken into accounts. Our recent developments based on correlation function or generating function by following the earlier work of Lax [34], Kubo [35] have been demonstrated very successful for complex molecules [36–40].

However, the non-radiative decay, especially the non-adiabatic decay of the lowest excited state to the ground state is far more complicated than the radiative decay process. Theoretically, this is a quantum dynamics problem for at least two potential energy surfaces. Though such a problem can only be solved for molecule with less than 4 atoms, there have been progresses made along this direction for complex systems [41–48]. However, so far, the non-adiabatic electron dynamics is limited to tens of picoseconds, suitable for studying the ultrafast conical intersection process with photochemical or biological interests. As far as light-emitting process is concerned, the radiative decay time ranges from millisecond (phosphorescence) to nanosecond (fluorescence). In the foreseeable future, quantum electron dynamics simulation is not expected to tackle this issue: the time step for electron dynamics simulation is usually attoseconds, and that for nuclear dynamics is about 0.1 femtosecond. There are from 9 to 12 orders of magnitude difference in timescale. This is a formidable challenge. Nevertheless, this issue has been tackled long back with physics model, for example, the Huang–Rhys formulation

of multiphonon non-radiative relaxation processes in 1950 [49], originally developed for the light-emitting from the color center in solids. The basic assumption is the Fermi-Golden rule for two quantum states modeled by displaced harmonic oscillator. In the 1960s, Lin [50], Jortner and others [51] further developed such formalism for molecular problems. Recent remarkable development has been along the line of correlation function formalism, which has been demonstrated to be both efficient and reasonably reliable [52]. Especially, such formalism has been extended by combining non-adiabatic coupling with spin–orbit coupling for treating both the radiative and non-radiative decays for phosphorescence [53]. We further consider the aggregation effects in this formalism and we found it can well account the recent discovered aggregation-induced emission (AIE) phenomena [54]. This will be introduced in Section 4.

2. Excited state ordering for extended chains — a density matrix renormalization group study

2.1. Introduction to DMRG: application to conjugated polymers

Density matrix renormalization group theory (DMRG) was first proposed by White for quantum system, which was demonstrated to have an unprecedented high accuracy when the real space renormalization scheme is carried out in the reduced density matrix Eigenspace. It systematically thins out of degrees of freedom leading to effective Hamiltonian. For many kind of materials, notably, the inorganic semiconductors with large dielectric constant $\varepsilon > 10$, the one-electron picture is very successful as the electronic structure can be ideally described by a band model. Organic materials usually have much lower dielectric constant ($\varepsilon \sim 2$–4), thus the Coulomb interaction in solid cannot be effectively screened out. Thus, DMRG is the most suitable method for conjugated polymers.

In a one-electron molecular orbital picture, the lowest excited state in polyenes is a single promotion of electron from HOMO to LUMO which is of odd-parity and dipole allowed, while the second lowest excited state is a linear combination of HOMO−1 to LUMO and HOMO to LUMO+1 which is of even-parity and dipole forbidden character. It is well established now that the electron correlation effect stabilizes the even parity state by mixing double excitation of HH->LL type, leading to the $2A_g < 1B_u$. This is based on the picture of configuration interaction derived from molecular orbitals. In real space, for a chain with N-site (atomic pi-orbital for carbon) and N pi-electron (half-filling), the atomic orbital can be empty, singly occupied with up or down electron, or doubly occupied. The probability for double occupation is 25% if there is not electron correlation. Hubbard introduced a penalty U for double occupation, allowing a minimum description of electron correlation effect yet exactly soluble [55–57]. For strongly correlated electrons ($U >> t$), the double occupied sites tend to be zero and the Hubbard model is equivalent to a $t-J$ model widely employed to study the cuprite superconductivity [58] and at half-filling to the Heisenberg model with spin half for magnetism. For $S = 1/2$ spin chain, the excitation is gapless according to Haldane conjecture [59]. That corresponds to a diminishing triplet excited state in molecule picture. It was also speculated that two triplet states form the $2A_g$ state [16], leaving it with very low excitation energy. At the same time, the dipole-allowed $1B_u$ excitation corresponds to one empty site and one doubly occupied site, which is stabilized by kinetic energy (moving electron and hole) but strongly destabilized by a positive U term.

Such a picture has been extensively employed by Soos, Mazumdar, Ramasesha et al. in emphasizing the electron correlation picture, [60–62] challenging the widespread single electron band picture. As far as exciton is concerned, there is a problem with the Hubbard U-only description, namely, the attraction term between electron and hole is missing in the Hubbard model. The minimum model to describe exciton binding along this line is to add a nearest-neighbor potential V, the extended Hubbard–Peierls model to study the exciton binding energy [63], excited state orderings and nonlinear optical responses in conjugated polymers, which reads:

$$H = -\sum_i t[1+(-1)^i\delta](c^+_{i\sigma}c_{i+1\sigma} + h.c.) + U\sum_i n_{i\uparrow}n_{i\downarrow} + V\sum_i (n_i-1)(n_{i+1}-1) \quad (1)$$

where t is the nearest neighbor pi-orbital hopping integral which stabilize charge transfer, δ is the dimensionless bond-length alternation parameters defined for alternating single-double bonds: $t(1+\delta)$ for double bond and $t(1-\delta)$ for single bond. U is the Hubbard's penalty for double occupation and V is the nearest neighbor Coulomb potential. Due to the complexity of both δ and V, this model cannot be solved exactly. Shuai et al. made further extension of Eq. (1) to a long-range Coulomb interaction potential [23] by replacing the last term by the Pariser–Parr–Pople (PPP) Hamiltonian: $\sum_{i<j} V(r_{ij})(n_i-1)(n_j-1)$ and $V(r)$ had been chosen as Ohno–Klopman type potentials. [64,65].

It was generally believed that the accuracy of DMRG drastically decreases for long-range interaction. For example, the 2-dimensional $t-J$ model designed for superconductivity was mapped to a 1-d chain with long range hopping term. The accuracy is no more guaranteed. [66] However, we found that by extension to the long range density–density interacting term, DMRG works very well. [67] One year later, Fano et al. independently worked out PPP model for the ground state of polyene with DMRG [68]. Then, a DMRG study for the general *ab initio* quantum chemistry Hamiltonian has been formulated by White and Martin [69]. These advances are now regarded as the start of quantum chemistry DMRG [70], an important field for accurate computation, largely enhancing the active space for multi-reference CI by Chan et al. [71].

The practice of DMRG for a linear chain electron system is the following: (i) starting from one site with Hilbert space of 4, namely, $|0\rangle$ for empty, $|\downarrow\rangle$ for down spin, $|\uparrow\rangle$ for up spin, and $|X\rangle$ for double occupation. All the quantum operators as well as Hamiltonian in Eq. (1) can be expressed as a 4×4. This is called a system, indexed by *i*. (ii) Then, we expand the

system by adding another site called environment, also with 4×4 space, indexed by i'. Now, the system plus environment consists of a direct product space with 16×16 dimension indexed by ii'. (iii) Since now the system and environment is the same (one site), we add one site both to the system and to the environment forming superblock of system (two sites σ and σ') and environment (two sites). The Hamiltonian equation (1) for the system plus environment now can be solved exactly giving the lowest Eigenstate as:

$$\psi_g = \sum_{i,j} c_{i\sigma\sigma' i'} |i\rangle|\sigma\rangle|\sigma'\rangle|i'\rangle. \tag{2}$$

Now the system is expanded from $|i\rangle$ to $|i\rangle|\sigma\rangle$. We can construct the reduced density matrix for the system as:

$$\rho_{i\sigma,j\tau} = \sum_{\sigma' i'} c_{i\sigma\sigma' i'}{}^* c_{j\tau\sigma' i'} \tag{3}$$

where $j\tau$ are the column indices for the Hilbert space of the new system. The reduced density matrix has the same dimension as the Hilbert space. Due to the normalization condition for $|\psi_g\rangle$, the trace of ρ is unity:

$$tr(\rho) = \sum_{i\sigma} \rho_{i\sigma,i\sigma} = \sum_{i\sigma\sigma' i'} c_{i\sigma\sigma' i'} c_{i\sigma\sigma' i'} = 1. \tag{4}$$

In other words, if we diagonalize ρ matrix, $O\rho O^+ = diag\{\lambda_1, \lambda_2, \ldots\}$ the sum of all the Eigenvalues should equal to 1 and since the reduced density matrix is positive definite, all the Eigenvalues are positive. It had been observed numerically that for one-dimensional short-ranged interacting model, the sum of very few Eigenvalues is already close to 1 and most Eigenvalues are practically zero, implying the Hilbert space is too much redundant for just describing the lowest-lying state or a few states. In fact, the expectation value of an operator A is simply $\bar{A} = tr(A\rho) = \sum_i A_{ii}\lambda_i$, implying the importance of keeping only a few largest λ will be sufficient to describe physical quantity. Then it was proposed to transform the Hilbert space to the Eigenvector space of the reduced density matrix for the system block (and for the environment block which are usually the same). Namely, all the operators as well as the Hamiltonian are transformed as: $\tilde{A} = OAO^+$, where matrix O is formed by the Eigenvectors of the density matrix. If all the Eigenvectors are kept, such transformation is canonical and equivalent. However, one can here introduce a cutoff value m. If we continue to add new site to the system and to the environment, the system space is expanded by 4 times for each added site until it reaches a cutoff value m. In this case, we keep only m Eigenvectors with the largest Eigenvalues. Keeping doing this operation, the system space goes from m to $4m$ and is cut back to m. This operation is continued until system plus environment reaches the targeted size N. The matrix representation of the Hamiltonian is expressed in the direct product space of the four blocks (left block, two sites, and right block):

$$\langle i\sigma\sigma' i'|H|j\tau\tau' j'\rangle = \langle i|H_L|j\rangle\langle\sigma|H_1|\tau\rangle\langle\sigma'|H_{1'}|\tau'\rangle\langle i'|H_R|j'\rangle. \tag{5}$$

Above renormalization procedure is termed as infinite-system algorithm. The final dimension of the Hamiltonian is $16m^2$, instead of 4^N. The advantage is that when enlarging the size, the environment contribution is always kept in the reduced density matrix by virtue of Eq. (2). This minimizes the boundary effect and consists of the essential advantage of DMRG over the traditional real space RG scheme. Once the desired size N is reached, the effective Hamiltonian can be even optimized by the "finite DMRG scheme": for a fixed length, $N = 2L + 2$, we continue to increase the system (left block) to $L + 1$ but at the same time to decrease the environment to $L - 1$ until we arrive at a point of $(2L - 1) + 1 + 1 + 1$. Then we sweep back by adding environment size until we come back at $L + 1 + 1 + L$. This is called one-sweep DMRG iteration. The iteration can be carried out for a few more times to further improve the accuracy. This refined basically every site with optimized basis.

2.2. Symmetrization of DMRG for fermion

In the above schemes, the symmetry consideration has been only for the total number of particles and the z-component of total spin (namely, the number of up spin minus the number of down spin). Ramasesha and co-workers have proposed a systematic symmetrization scheme in DMRG [22]. Since for conjugated polymers, people are mostly interested at half-filling case. Therefore, for Eq. (1), there are at least the inversion, electron–hole symmetry (half-filling), and spin up–down symmetry (half-filling also). The spatial inversion operation classifies the space into A and B. Charge conjugation allows labeling '+' for covalent and '−' for ionic space. And spin up/down divides states into odd ('o') total spin $S = 1, 3, 5, \ldots$ and even ('e') total spin $S = 0, 2, 4, \ldots$, though not total spin itself which requires Clebsch–Gordon coefficient to combine different blocks, which was not implemented.

The charge-conjugation operator (J) interchange, with a phase, the creation and annihilation operators at a site i, such that $J_i|0\rangle = |X\rangle, J_i|\uparrow\rangle = (-1)^i|\uparrow\rangle, J_i|\downarrow\rangle = (-1)^i|\downarrow\rangle, J_i|X\rangle = (-1)|0\rangle$. The total operation is a direct product of all the sites $J = \prod_i J_i$. The spin parity operation (P) at a site i flips its spin: $P_i|0\rangle = |0\rangle, P_i|\downarrow\rangle = |\uparrow\rangle, P_i|\uparrow\rangle = |\downarrow\rangle, P_i|X\rangle = -|X\rangle$, where the minus sign comes from the up–down electron commutation. The total parity operation is a product of all the sites $P = \prod_i P_i$. C_2 symmetry interchanges the states of the left and right halves of the system with a phase factor:

$$C_2|i, \sigma, \sigma', i'\rangle = (-1)^{(n_i + n_\sigma)(n_{i'} + n_{\sigma'})}|i', \sigma', \sigma, i\rangle. \tag{6}$$

These three operations are independent and commute each other. The combinations form an Abelian group with eight elements and the eight irreducible representations are labeled as ${}^eA^+$, ${}^eA^-$, ${}^oA^+$, ${}^oA^-$, ${}^eB^+$, ${}^eB^-$, ${}^oB^+$, and ${}^oB^-$. The symmetry projection operator for a given irreducible representation Γ is given by:

$$\hat{P}_\Gamma = \frac{1}{h}\sum_{\hat{R}} \chi_\Gamma(\hat{R})\hat{R}. \tag{7}$$

Here, $h = 8$ is the order of the group, R is the symmetry operator, and χ is the corresponding character ($+1$ or -1 here). The symmetry adaptation is obtained by operating Eq. (7) to all the Hilbert basis $|i, \sigma, \sigma', i'\rangle$. By eliminating the linear dependence of the resulting basis, we obtained the symmetrization matrix for transforming the unsymmetrized basis to the symmetrized basis. This matrix is again expressed as a direct product of four blocks:

$$\langle i, \sigma, \sigma', i'|S_{2l+2}|j, \tau, \tau', j'\rangle = \langle i|S_L|j\rangle\langle\sigma|S_1|\tau\rangle\langle\sigma'|S_{1'}|\tau'\rangle\langle i'|S_R|j'\rangle \tag{8}$$

exactly as the structure of Hamiltonian matrix. This is possible since our symmetry operation is done locally on site. The symmetrization matrix is renormalized at the same time as the Hamiltonian matrix, $\tilde{S}_{l+1} = O^+ S_{l+1} O$.

Eventually, the total Hamiltonian matrix in the direct product space is transformed into the symmetrized basis by $\tilde{H}_{2l+2} = S^+_{2l+2} H_{2l+2} S_{2l+2}$ for specific irreducible representation, which is readily to be diagonalized by a Davidson algorithm. For the Hubbard model, numerical calculation gives an ordering ${}^eA^+ < {}^oA^+ < {}^oB^+ < {}^eB^+ < {}^eB^- < {}^eA^- < {}^oB^- < {}^oA^-$.

The symmetrization does not decrease the computational cost, even though the final effective Hamiltonian matrix dimension is reduced, since we need to work in both the unsymmetrized and the symmetrized spaces. However, since in DMRG, the renormalization is carried for a target state by which we built the reduced density matrix according to Eq. (2), the symmetrization is especially useful for targeting the excited state by working on the specific symmetrized space. For example, the optically allowed states should have symmetry ${}^oB^-$ due to the nature of the electric dipole operator. If we target the ground state, the renormalized basis do not contain enough space for expressing the excited state. However, if we target the lowest state within the ${}^oB^-$ subspace, the resulting effective Hamiltonian can capture most of the excited state components. If there is no cutoff, the two schemes give the same results.

2.3. Low-lying excited state orderings in conjugated chains

The low-lying excited state orderings is the first criterion for judging the luminescence. Correlated electron systems possess very different electronic structure from the single electron systems. For short polyene, HOMO to LUMO single excitation is notably larger than the HOMO to LUMO+1 excitation ($1B_u < 2A_g$). Once electron correlation turns on, the ordering is reversed. It was found from exact diagonalization that the critical correlation strength for such ordering crossover occurs at $U/t \sim 2.5$. The physical reason for such crossover is that the ionic $1B_u$ state increases with U, and the covalent $2A_g$ state decreases with U because it is mostly composed of spin excitation which is gapless in strong correlation limit. For an infinite long chain, the single-electron picture should present almost degenerate $1B_u$ and $2A_g$, since the difference between LUMO and LUMO+1 is negligible. The crossover behavior can only be investigated with the symmetrized DMRG, since we should deal with large correlated electron systems. [72] In the conventional DMRG, it is difficult to target $1B_u$ state, since there are many states between it and the ground state and the number increases with both chain length and the correlation strength. Exploiting spin parity, C_2, and the charge conjugation, $1B_u$ state is simply the lowest state in the specified subspace. The $2A_g$ state also becomes easier to be targeted since many intruder states have been singled out by symmetry operation. Thus, we are able to contrast the excited state ordering for short chain ($N = 8$) to that of long chain ($N = 80$), which is shown in Fig. 1 for a bond alternation parameter $\delta = 0.07$. The DMRG cutoff has been chosen between $m = 100$ and $m = 150$, depending on the necessity of numerical convergence at about 10^{-5}. Since our parameters correspond to moderate correlation (U/t up to 5), realistic to conjugated polymers, the picture is quite different from the strong correlation. First we note that the $1B_u$ increases steadily with U as expected. However, the $2A_g$ state at lower U increases with U first, and then levels off, and then decreases with U. Surprisingly, the crossover of $1B_u$ and $2A_g$ occurs at the almost the same U value around $U/t \sim 2.5$.

Soos et al. have first demonstrated a crossover on δ, namely, there exists a critical δ_c, below which the $2A_g$ is below $1B_u$ (no light emitting), and above which $2A_g$ is destabilized to be above $1B_u$ [73]. In fact, for larger δ, there are more ionic components in $2A_g$. Our DMRG reproduces well the previous finding of such crossover. However, we have demonstrated a novel type of crossover, the chain length crossover. This is based on our numerical experiment that the critical δ_c depends on chain length. Longer chain possesses a smaller δ_c. Thus, for δ value between the δ_c of long chain and short chain, there must occur a crossover with chain length, see Fig. 2. In other words, there should exist parameter windows within which for short chain $2A_g$ is below $1B_u$ (non-emissive), but for longer oligomers, $1B_u$ is stabilized to be below $1B_u$ and emission can be recovered.

It should be noted that such crossover is not universal, because the parameter window is narrow. For instance, for polyacetylene, $\delta = 0.07$, for both short and long chains, the $2A_g$ is always below $1B_u$. Nevertheless, Fig. 2 simply indicated such possibility. There existed experimental evidence that light-emitting behavior vary with the length of oligomers [74].

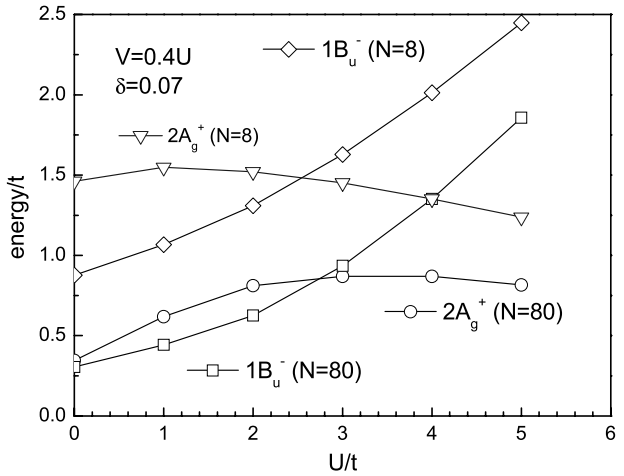

Fig. 1. Evolution of $1B_u$ and $2A_g$ state energy with U for polyene $N = 8$ and $N = 80$.
Source: Reprinted figure with permission from Ref. [72].

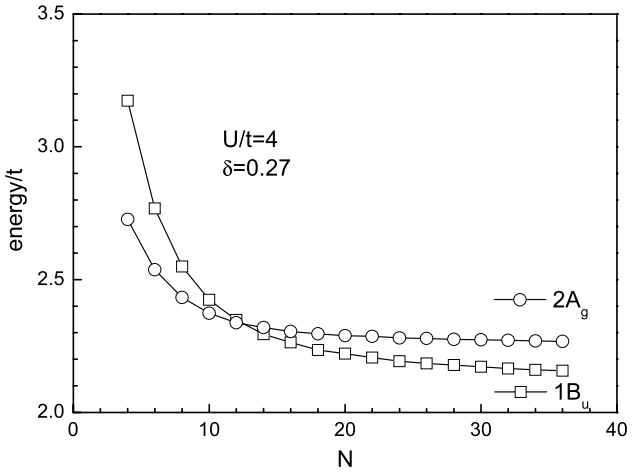

Fig. 2. Excited state ordering crossover with respect to chain length.
Source: Reprinted figure with permission from Ref. [72].

Table 1
Low-lying excited state energy calculated by symmetrized DMRG for polyenes ($N = 4$–30) with PPP model/Ohno potential.

N	4	6	8	10	12	14	16	18	20	22	24	26	28	30
$1B_u$	5.84	5.05	4.56	4.23	3.99	3.82	3.69	3.59	3.51	3.45	3.39	3.35	3.32	3.29
$2A_g$	5.33	4.35	3.74	3.35	3.09	2.92	2.79	2.70	2.63	2.58	2.55	2.52	2.50	2.48

The above results have been based on an extended Hubbard model with U and V-terms. In order to better compare with quantum chemistry, we present the results for Ohno potential. For polyacetylene, the parameters were the same as previous work: $U = 11.26$ eV, $t = -2.4$ eV, $\delta = 0.07$, and the bond-lengths for single and double bonds are 1.45 and 1.36 Å. For such fully long ranged potential, DMRG can be still regarded as nearly exact, in the sense that (i) when increasing the cut-off dimension m from 100 to 120, the ground state total energy per electron is lowered only 10^{-3} eV; (ii) for $m = 100$, the difference between 1 and the sum of the kept density matrix Eigenvalues is less than 10^{-5}, which is widely regarded as the criterion for DMRG accuracy. We plot the $1B_u$, $2A_g$ and twice of T_1 state energies in Fig. 3. As is seen, $2A_g$ is below $1B_u$ for all lengths except for $N = 4$, in agreement with experiments, and $2A_g$ is indeed close to twice of the T_1 state energy. The numerical values are given in Table 1.

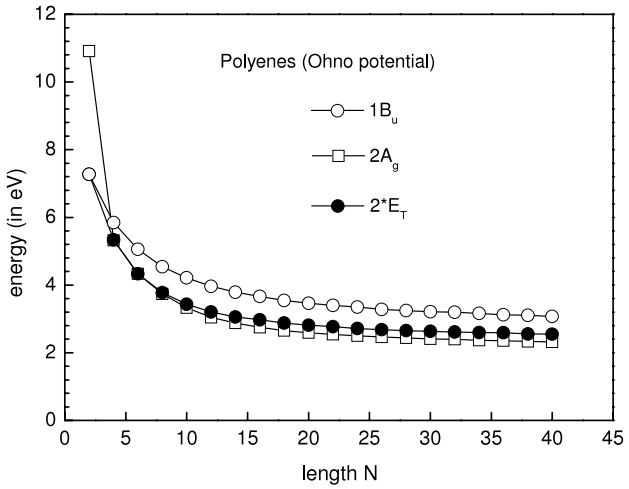

Fig. 3. Evolution of $1B_u$, $2A_g$, and twice of the lowest triplet states as a function of polyene length from DMRG calculation for the PPP model. *Source:* From Ref. [23].

Table 2
$1B_u$ and $2A_g$ states energy (in eV) calculated at the EOM/CCSD level with INDO parameterization for native (−H) and substituted oligo-diacetylenes.

R	*n*	1	2	3
−H	2^1Ag	5.601	4.255	3.972
	1^1Bu	5.286	4.520	4.109
$-CH_3$	2^1Ag	5.617	4.256	4.011
	1^1Bu	5.222	4.473	4.088
$-OCH_3$	2^1Ag	5.260	3.696	3.394
	1^1Bu	4.945	4.186	3.709
−CHO	2^1Ag	5.055	3.570	3.382
	1^1Bu	4.182	3.696	3.398
−CN	2^1Ag	5.215	3.642	3.427
	1^1Bu	4.470	3.853	3.508

2.4. Altering excited state ordering by molecular design

So far we understand the origin of crossover behavior. Namely, $1B_u$ is ionic state while $2A_g$ consists of mainly covalent excitation. Electron correlation effect governs the ordering while chemical structure and even conjugation length also play important roles. Chemical substitutions are effective molecular design methods. For non-emissive polymers, side-chain substitution can result in charge modification for the main to stabilize the $1B_u$ state. In fact, even for polyacetylene, there have been successful examples for substitution induced light-emitting [75]. The question we like to address here is can we predict what types of side-chain substitution can lead to excited state ordering alteration? We carry out a case study for non-emissive polydiacetylene (PDA) (see Fig. 4). Despite of controversies over the nature of the lowest-lying excited state in PDA in both experiment and theory, more and more experimental evidences indicated that $2A_g$ is the lowest-lying excited state in PDA [76]. PDA has been the only polymer which can be crystallized in large scale thus possessing large carrier mobility [77,78]. To achieve electrical pump lasing, both light-emitting and large mobility are required. It is thus of important interests to design PDA to be highly emissive.

The substitution effect could be modeled by introducing site-energy term in the main chain. However, the parameterization is not an easy task, which could lead to arbitrary conclusion regarding the excited state structure. We thus resort to quantum chemistry with well-defined model. Since from the PPP model, the bond alternation parameter δ for PDA is small, which does not fall in the window of any chain length dependent crossover region, we then can use short chain oligomers, which are tractable by quantum chemistry with correlated electrons, such as equation of motion coupled cluster method. We resorted to an Incomplete Neglect of Diatomic Orbital (INDO) parameterized version of home-made EOM/CC program [16], which can capture the essential features for electron correlation as well as for conjugated structure. In Table 2, we present the calculated excited states energy for the native and substituted PDA oligomers. It is seen that chemical substitution cannot alter the ordering, namely, in all the cases, we always have $2A_g < 1B_u$. This predicted that it is almost impossible to modify PDA to be light-emitting.

We carried out more calculations on other diacetylene derivatives such as 1, 4-pentadiyne and p-phenylenebutadiynylene oligomers [79], where in some cases, we did find that substitution can cause the excited state ordering alterations.

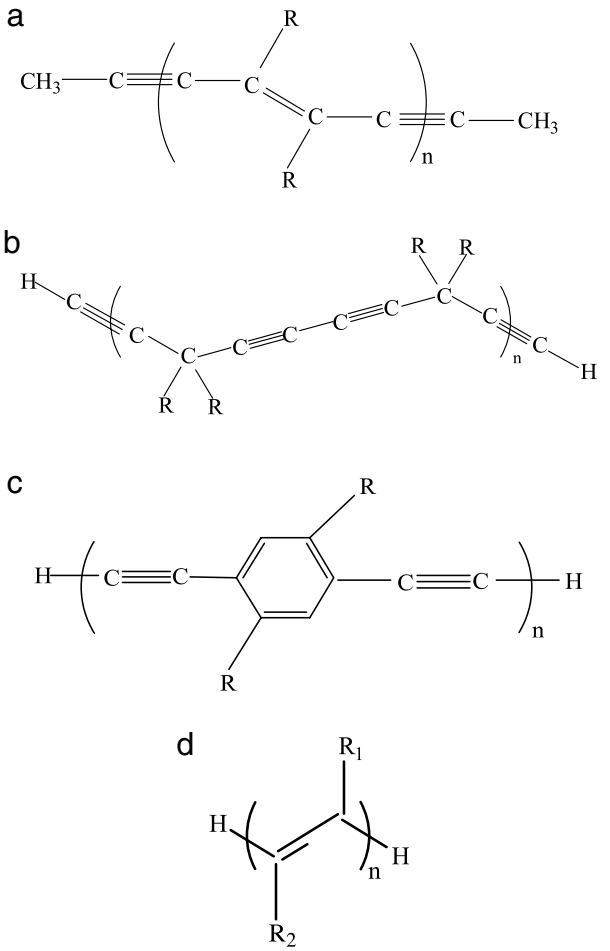

Fig. 4. Chemical structures of the substituted PDA and derivatives and PA.
Source: Reprinted figure with permission from Ref. [79].

Since such calculations involve complicated method with electron correlation, we intended to propose a simple rule to judge the ability for substitution induced state alteration. We define the following quantity:

$$\rho_{H/L} = \frac{\sum_{\mu \in sub} \left| C_{H\mu} \right|^2}{\sum_{\mu \in sub} \left| C_{L\mu} \right|^2} \tag{9}$$

where $C_{H(L)\mu}$ is the molecular orbital coefficient of HOMO (LUMO) at atomic orbital μ. The summation is only carried out for atomic orbitals in the polymer backbone linking with the substituents. $\rho_{H/L}$ can characterize the induced charge density modifications between the HOMO and LUMO. This is because that the ionic $1B_u$ state consists of mostly a transition from HOMO to LUMO. For conjugated polymer, if the overall electron densities for the HOMO and LUMO are similar, then $\rho_{H/L}$ should be close to 1. In another word, the substitution does not cause much effect on the charge distribution character in the $1B_u$ state for the main chain. Namely, the substitution is not expected to alter the ordering of the $1B_u$ state with respect to other excited states. Otherwise, if the quantity $\rho_{H/L}$ is well away from 1, then, it means that there may cause charge transfer from the substitute moiety to the main chain part. That is to say, that the substitution is expected to induce charge redistribution in the lowest-lying excited state structure, which stabilize the ionic $1B_u$ state while leave the covalent $2A_g$ untouched.

Indeed, this simple rule does work. We present in Table 3 the calculated results for $\rho_{H/L}$ for all the substituted compounds. We are able to observe that in all cases, if $\rho_{H/L}$ is close to 1, the substitution effects do not alter the ordering of $1B_u/2A_g$; and if $\rho_{H/L}$ is well away from 1, either much larger than or much less than 1, then $1B_u$ state becomes the lowest excited state. Thus, we can easily classify the emissive and non-emissive materials according to $\rho_{H/L}$.

Table 3
The ratio $\rho_{H/L}$ for all the compounds investigated in this work, which are classified into two categories: $2A_g < 1B_u$ and $2A_g > 1B_u$. In the former group, the $\rho_{H/L}$ is usually close to 1, while in the latter group, $\rho_{H/L}$ is usually either much larger or much less than 1.

$2A_g < 1B_u$				$2A_g > 1B_u$			
Compound(a)		Compound (d)		Compound (b)		Compound I	
R = CH_3, N = 2	0.90	R = CH_3, N = 2	0.94	R = CH_3, N = 1	8.33	R = CH_3, N = 2	1.34
R = CH_3, N = 3	0.92	R = CH_3, N = 3	0.96	R = CH_3, N = 2	4.77	R = CH_3, N = 3	1.29
R = OCH_3, N = 2	0.97	R = CH_3, N = 4	0.96	R = CH_3, N = 3	4.29	R = CH_3, N = 4	1.27
R = OCH_3, N = 3	0.99	R = OCH_3, N = 2	0.81	R = OCH_3, N = 1	1.21	R = OCH_3, N = 2	2.31
R = CHO, N = 2	0.79	R = OCH_3, N = 3	0.86	R = OCH_3, N = 2	1.32	R = OCH_3, N = 3	2.09
R = CHO, N = 3	0.80	R = OCH_3, N = 4	0.88	R = OCH_3, N = 3	1.33	R = OCH_3, N = 4	2.02
R = CN, N = 2	0.76	R = CN, N = 2	0.86	R = CHO, N = 1	4.18	R = $COOCH_3$, N = 2	0.27
R = CN, N = 3	0.78	R = CN, N = 3	0.89	R = CHO, N = 2	6.51	R = $COOCH_3$, N = 3	0.30
		R = CN, N = 4	0.90	R = CHO, N = 3	–	R = $COOCH_3$, N = 4	–
				R = CN, N = 1	14.45		
				R = CN, N = 2	11.03		
				R = CN, N = 3	–		

3. Spin-dependent exciton formation in polymer electroluminescence

3.1. Electronic coupling consideration — interchain bond-charge correlation

The fundamental electronic processes in polymer light-emitting diodes consist of charge injection from electrodes to polymers, charge transport in the active polymer semiconductors, charge recombinations, and excitation decay. We aim to address at the molecular level the nature of the main parameters that govern electron-recombination processes in oligomer and polymer LEDs. We investigate the spin-dependent exciton formation rates in polyparaphenylenevinylene chains and their evolutions with the chain length. The quantum efficiency of organic light-emitting diodes depends to a large extent on the nature of the exciton which is a function of both electron-vibration and electron–electron interactions [80]. The exciton binding energy falls in a few tenth of an eV [81]. Singlet and triplet excitons possess different energies, with difference, that is the exchange energy, estimated to be larger than half an eV for the lowest excitation in a range of conjugated polymers [82–85]. They also display different geometry relaxations; due to the possibility of exchange between like spins, triplet wavefunctions usually display a more spatially confined character, a feature that is especially pronounced for low-lying excitations [86].

The quantum efficiency for electroluminescence (photoluminescence), $\eta_{EL}(\eta_{PL})$, is defined as the ratio between the number of photons coming out of the device and the number of electrons injected (photons absorbed). In π-conjugated oligomers and polymers, the ratio η_{EL}/η_{PL} is controlled by the fraction of singlet excitons generated in the diode (hereafter referred to as η_2). For a long time, this ratio was thought to follow simple spin multiplicity rules according to which η_{EL}/η_{PL} should not exceed 25% (since the recombination of an electron–hole pair — both spin $\frac{1}{2}$– leads to a total of four microstates with three triplet states and one singlet state).

It must be clearly stated that this issue remains controversial [87] even if there existed some compelling experimental [29,88–93] and theoretical [30,94–98] evidences that, in conjugated polymers, larger ratios than 25% between EL and PL quantum yields can be achieved. This stresses the possibility of producing highly efficient polymer LEDs and raises fundamental questions about the mechanisms determining exciton formation, which we now review.

Cao et al. found that upon improving the electron transport properties of a substituted poly(paraphenylenevinylene)-based LED device, the ratio of external quantum efficiencies of EL with respect to PL can reach a value as high as 50% [29]. Values of η_2 ranging from 0.35 to 0.45 have also been reported by Ho et al. in PPV derivatives [88]. Wohlgenannt et al. have measured η_2 by using a photo-induced absorption detected magnetic resonance (PADMR) technique for a large number of π-conjugated polymers and oligomers; the experimental η_2 values were found to increase with conjugation length ranging from ∼0.25 in monomers to much larger values in extended π-conjugated systems [90]. Similarly, Wilson et al. have reported a singlet generation fraction close to 57% in a platinum-containing conjugated polymer, while a much smaller value (22%) was inferred for the corresponding monomer [89]. A work reported by Philips was especially important in this regard and suggested the quantum yields on the order of 60% in polymer LEDs based on polyparaphenylene vinylene or polyspirobifluorenes [93]. From these experimental data, the emerging picture is that η_2 follows closely spin statistics in small conjugated oligomers or molecules [99] while the 25 % statistical limit can be significantly overcome in polymers.

Charge recombination between an injected electron and an injected hole occurs as a two-step process [92]. First, the initially fully separated charges coalesce into loosely-bound singlet or triplet polaron pairs, also referred to as charge-transfer (CT) excitons. In a second step, these intermediate states then decay into lower bound singlet or triplet (exciton). Two major aspects need to be emphasized: (i) since in the first step, spin statistics is always obeyed, if the second step is faster than any other process affecting the intermediate CT states, spin statistics will be followed eventually. Thus, overcoming spin statistics requires that the second step be significantly slower for triplet than for singlet CT states. There are two scenarios to break down the spin statistics: either intersystem crossing can switch triplet pairs into singlet pairs [100,101] that could decay down in the singlet exciton manifold; or triplet pairs can have time to dissociate and some of the freed charges can later

recombine as singlet pairs. (ii) Kadashchuk et al. [102] have carried out a thermoluminescence measurements on ladder-type phenylene-based polymers. They found that the singlet–triplet splitting among the interchain CT states is merely on the order on 3–6 meV, allowing intersystem crossing or dissociation of the CT states.

If we denote by σ_S and σ_T the cross-sections for formation of neutral singlet and triplet exciton states, the expression for $\eta_2$can be written as:

$$\eta_2 = \sigma_S/(\sigma_S + 3\sigma_T) = \sigma_{S/T}/(\sigma_{S/T} + 3) \tag{10}$$

where $\sigma_{S/T} = \sigma_S/\sigma_T$. For $\sigma_S = \sigma_T$, we get $\eta_2 = 25\%$, the statistical limit; η_2 becomes 50% for $\sigma_S = 3\sigma_T$; for $\sigma_T = 0$, $\eta_2 = 100\%$.

Theoretically, Shuai et al. first suggested that the interchain charge recombination to form exciton is a spin-dependent process [30,94]. The origin of such dependence is from the electronic coupling term when the interchain electron correlation involves off-diagonal term, of the type of $[\mu\mu|\mu\nu]$. Bittner and co-workers have simulated the dissipative dynamics of an extended one-dimensional polymer system coupled to a phonon bath [95,96]. When applying this formalism to a quantum molecular dynamics simulation of the formation of exciton states from polaron pairs, they found a clear correlation between the rates for intrachain generation of singlet and triplet excitons on a single long PPV segment and the corresponding binding energy: the ratio σ_s/σ_T was calculated to evolve linearly with the singlet to triplet binding energy ratio [95]. This evolution was explained in terms of spin specific energetics and mutual vibronic couplings between the excited states on an isolated polymer chain. We argued that the rate limiting step is the interchain charge recombination process from the CT states into the manifold of intrachain singlet and triplet excitons, followed by faster downhill internal conversion driven by vibronic couplings. Mazumdar and co-workers also reported chain-length dependent formation cross-sections for interchain charge recombination, based on exact calculations for small polyene chains [97].

For both charge transfer and the energy transfer processes, the interchain channel is dominant since the intrachain process is too fast and the overall efficiency is controlled by the much slower interchain ones. In such situation, the Fermi Golden Rule is appropriate to apply.

$$k_{if} = \frac{2\pi}{\hbar}|\langle\psi_i|V|\psi_f\rangle|^2\rho(E_f) \tag{11}$$

where i represents the initial state and f the final state, V is electronic coupling depending on the nature of process, and ρ is the density of state (DOS). For both charge and energy transfers, the transition mechanisms involve vibrational motions driving the reaction coordinates from reactants to products. We emphasize that the charge recombination should be a bi-molecular process. So we introduced a general interchain interaction perturbation term including both one-electron and two-electron terms:

$$H' = \sum_{pq} h_{pq}p^+q + \frac{1}{2}\sum_{pqsr}\langle pq|rs\rangle p^+q^+sr. \tag{12}$$

Each has a mixing of chain 1 and 2 spin–orbital indices: h_{pq} is the interchain hopping integral $h_{pq} = \sum_{\mu_1\nu_2} t^{\perp}_{\mu_1\nu_2}\psi_{p\mu_1}\psi_{q\nu_2}$ and $\langle pq|rs\rangle = \sum_{\mu\nu\sigma\tau}\psi_{p\mu}\psi_{q\nu}\psi_{r\sigma}\psi_{s\tau}[\mu\sigma|\nu\tau]$ is the interchain Coulomb integral. It is always reasonable to assume that the exciton is localized on a single polymer chain. Under the configuration interaction with single (CIS) excitation description, the spin-adapted exciton state is expressed as:

$$|x1\rangle = \frac{1}{\sqrt{2}}\sum_{i_1a_1} Z_{i_1a_1}(a_{1\uparrow}{}^+i_{1\downarrow} \pm a_{1\downarrow}{}^+i_{1\downarrow})|0\rangle \tag{13}$$

where index 1 is for chain 1, a for virtual and i for occupied orbitals, $|0\rangle$ for Hartree–Fock single reference determinant, and Z is the CIS coefficient. The initial state to describe the electroluminescence is a CT state:

$$|in1\rangle = \frac{1}{\sqrt{2}}(L_{2\uparrow}{}^+H_{1\uparrow} \pm L_{2\downarrow}{}^+H_{1\downarrow})|0\rangle. \tag{14}$$

In both Eqs. (13) and (14), + and − in the combination represents spin singlet and triplet, respectively. And in Eq. (14), L is for LUMO (electron injection) and H for HOMO (hole injection). So Eq. (14) is a CT state with hole on chain 1 and electron on chain 2. When evaluating $\langle x1|H'|in1\rangle$, it can be shown that the only contribution from the two-electron term is the non-diagonal Coulomb integral of the type (11|12) or (22|21), or interchain charge-bond interaction, which had been found to play important role for polymer dimerization [103] and in photo-induced charge transfer process [104]. In parallel to one-electron integral termed as $t^{\perp}$, we term such off-diagonal integral as $X^{\perp}$ for the closest pair of interchain atomic orbitals:

$$\langle x1|H'|in1\rangle = \sum_{a_1} Z_{H_1a_1}\sum_{\mu_1\nu_2}\psi_{a_1\mu_1}\psi_{L_2\nu_2}(t^{\perp}_{\mu_1\nu_2} + X^{\perp}_{\mu_1\nu_2}) \pm \sum_{i_1a_1} Z_{i_1a_1}\sum_{\mu_1\nu_2}\psi_{a_1\mu_1}\psi_{H_1\mu_1}\psi_{i_1\mu_1}\psi_{L_2\nu_2}X^{\perp}_{\mu_1\nu_2}. \tag{15}$$

Immediately, we see that first-order perturbation for the charge recombination rate (electronic coupling term) depends on the spin manifold. The origin of the difference arises from the off-diagonal interchain bond-charge correlation $X^{\perp}$. We have performed *ab initio* quantum chemistry calculation for butadienes dimer cofacially separated by 4 Å with the minimal basis. It is found that the $X^{\perp}$ is about one fourth of $t^{\perp}$. This is a non-negligible effect.

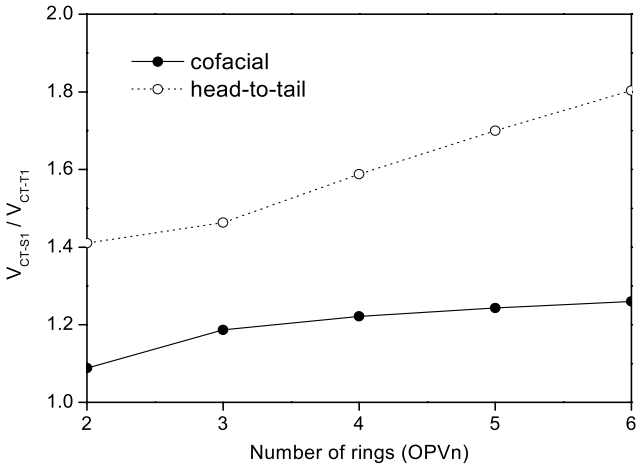

Fig. 5. Evolution with chain length of the ratio between the exciton formation electronic couplings, V_{if}, into the lowest singlet and triplet excited states, in cofacial (solid line) and head-to-tail (dashed line) configurations.
Source: Reprinted figure with permission from Ref. [105].

3.2. Driving force makes difference in the charge recombination process

Further, we take PPV oligomer dimer and compare from $N = 2$ (trans-stilbene) to $N = 6$. We consider two typical dimer stacking modes: cofacial (H-aggregate) and head-to-tail (J-aggregate). Quantum chemistry calculation based on PPP Hamiltonian showed that the electronic coupling (between CT state and the lowest exciton state) ratio of singlet with respect to triplet manifold is consistently higher than 1, see Fig. 5, in consistency with the butadiene dimer case.

The above discussion was based on only the electronic coupling term, namely, the electron tunneling between two polymer-chains, or the prefactor in Eq. (11). Beljonne et al. [105] had further considered the density of states term in Eq. (11) by employing a charge transfer formula [106] to estimate the charge recombination rates for singlet and triplet exciton formation. It was found that : (i) k_S/k_T ratio is smaller or close to one for short chain ($N = 2$) oligomer, while it is much higher in long chain ($N = 6$); (ii) in spite of the relatively small electronic couplings, the calculated recombination rates at room temperature are relatively fast: in $N = 2$, on the order of 10^9–10^{10} s^{-1} for both singlets and triplets; in $N = 64$, ca. 10^{10}–10^{11} s^{-1} for singlets but significantly smaller, 10^7–10^8 s^{-1}, for triplets.

So far, we have proved the principle that the conventional wisdom of spin statistics can be beaten. Namely, the internal quantum efficiency for organic electroluminescence can exceed the believed 25% ! The key issue here is that the charge recombination process falls in the Marcus inverted regime that the larger the driving force, the slower the charge transfer rate. In order to provide deeper insight and simpler clues for highly efficient light-emitting materials design, we may write down a simple relation from the Fermi Golden Rule, for the formation probability from an initial state (the free charge pair) to a final state (the bound ionic exciton) as:

$$p = \left| \frac{\langle i| H' |\rangle \sin(\omega_{fi} t/2)}{E_i - E_f} \right|^2 \tag{16}$$

where p represents the exciton formation probability. The formation rate is the time derivative of the above quantity:

$$\sigma = \frac{dp}{dt} = \frac{\left|\langle i| H' |\rangle\right|^2 \sin\left(\omega_{fi} t\right)}{2\hbar E_{fi}}. \tag{17}$$

Thus, apart from the prefactor as well as the time oscillation, the ratio of singlet exciton formation rate with respect to the triplet is simply expressed as [107–109]:

$$r_{S/T} = \frac{\sigma_S}{\sigma_T} = \left(\frac{E^T_{CT} - E_{T1}}{E^S_{CT} - E_{S1}}\right) = \left(\frac{E^T_b}{E^S_b}\right) \tag{18}$$

where E_b is the binding energy of exciton (difference between CT state and the exciton state in the respective spin manifold). These quantities are sensitive to the chemical structure of materials as well as external electric field. Such approximate and simple relation is helpful for molecular design. Namely, for a given material, the ratio of singlet exciton is determined by the singlet exciton binding energy and the singlet–triplet splitting, by which Eq. (18) is rewritten as:

$$r_{S/T} = \frac{E^S_b + \Delta_{ST}}{E^S_b} = 1 + \frac{\Delta_{ST}}{E^S_b} \tag{19}$$

Table 4
Singlet and triplet excitation energies (in eV) for the oligomers and polymers. Column 1 indicates the oligomers ($n = 2$, 3, 4, 5) and the polymer ($n = \infty$) for different materials. The calculated singlet and triplet excitation energies through INDO/CCSD-EOM for the oligomers and polymers are listed in column 2 and 4, respectively. The available experimental singlet and triplet values are listed in columns 3 and 5 for comparison.

PEDOT	Calc. (S)	Exp. (S)	Calc. (T)	Exp. (T)	MEHPPV	Calc. (S)	Exp. (S)	Calc. (T)	Exp. (T)
$n = 2$	3.83	3.87	1.56		$n = 2$	4.08		2.74	
$n = 3$	3.28	3.10	1.27		$n = 3$	3.61		2.52	
$n = 4$	2.97		1.13		$n = 4$	3.34		2.33	
$n = 5$	2.78		1.05		$n = 5$	3.25		2.17	
$n = \infty$	2.09	1.60	0.70		$n = \infty$	2.66	2.48	1.85	1.30
PTV					PPV				
$n = 2$	3.79	3.45	1.69	1.52	$n = 2$	4.48	4.01	2.40	2.13
$n = 3$	3.25	2.85	1.39	1.32	$n = 3$	3.83	3.44	2.37	
$n = 4$	3.00	2.56	1.27	1.23	$n = 4$	3.61	3.20	2.23	
$n = 5$	2.87		1.25		$n = 5$	3.51	3.07	2.17	
$n = \infty$	2.24	1.80	0.91		$n = \infty$	2.80	2.45	2.05	
PT					PPE				
$n = 2$	4.04	4.05	1.85	2.23	$n = 2$	4.83		3.29	
$n = 3$	3.55	3.49	1.52	1.93	$n = 3$	4.28		3.26	
$n = 4$	3.28	3.16	1.36	1.81	$n = 4$	4.03		3.11	
$n = 5$	3.09	2.99	1.27	1.72	$n = 5$	3.90		3.05	
$n = \infty$	2.48	2.20	0.89		$n = \infty$	3.26	3.20	2.92	
mLPPP					PFO				
$n = 2$	3.88	3.30	2.64	2.23	$n = 2$	4.13		2.77	
$n = 3$	3.72		2.57		$n = 3$	3.88	3.56	2.66	
$n = 4$	3.56		2.52		$n = 4$	3.77	3.43	2.56	
$n = 5$					$n = 5$				
$n = \infty$	3.27	2.72	2.41	2.08	$n = \infty$	3.40	3.22	2.36	2.30

where Δ_{ST} is the singlet–triplet splitting energy. Through quantum chemistry calculation, we first look at this ratio as a function of polymer structure [109]. Wohlgenannt et al. have measured a series of semiconducting polymers and plotted the ratio $r_{S/T}$ as a function of the optical gap [110]. This measurement has been questioned by Segal et al. [87,111] and Reufer et al. [112]. The latter claimed that in both small molecule like Alq_3 and conjugated polymers, the electro-excited singlet exciton portion cannot exceed the 25% spin statistical limit.

We employed the coupled-cluster equation of motion (EOM/CC) for semiempirical INDO model Hamiltonian to calculate the lowest singlet and triplet excited states [109] for polythiophene (PT), poly(3,4-ethylenedioxythiophene) (PEDOT), poly(thienylenevinylene) (PTV), polyparaphenylene vinylene (PPV), MEHPPV, polyparaphenylene ethylene (PPE), polyfluorene (PFO), and ladder-type polyparaphenylene (mLPPP). The results for the polymer are extrapolated through computations for the oligomers with increasing length. The computational results are depicted in Table 4, in comparison with the available experimental values. We find that the deviation of the calculated values from experiments is 0.29 eV for oligomers and 0.32 eV for polymers, which is acceptable when comparing with the state-of-the-art quantum chemistry methods for large system. Moreover, we find that the trend of optical gap is fully in agreement with experiment, that is, PEDOT $<$ PTV $<$ PT $<$ MEHPPV $<$ PPV $<$ PPE $<$ mLPPP $<$ PFO. Δ_{ST} is calculated from the difference of the extrapolated polymer singlet and triplet excitation energies.

The singlet exciton binding energy (E_b) for conjugated polymers is another long-standing controversial issue in this field. It has been claimed that E_b should be less than room temperature for PPV since the onset of photocurrent coincides well that of optical absorption, among other reasons [113], namely weakly bound e–h pair. Transient nonlinear optical detection also claimed that E_b should be larger than 0.85 eV for different reasons including the detection of $2A_g$ state and another onset of giant photocurrent in much higher energy [114], namely strongly bound e–h pair. More electrical and optical measurements showed that for most of the light-emitting polymers, E_b is the vicinity of 0.4∼0.5 eV [115,116], namely, intermediately bound e–h pair. From a DMRG "nearly" exact solution, we have lent support for the intermediate exciting binding regime [63]. Here, for simplicity, we assume an exciton binding energy of 0.5 eV for all the light-emitting polymers studied here. Now, using Eq. (19) and Table 4, we can plot the singlet/triplet formation ratio as a function of optical excitation gap, see Fig. 6, in comparison with the measurement of Wohlgenannt et al. [110]. The overall tendency agrees well with the experiment, providing further evidences to clarify this highly controversial issue.

3.3. Recent experimental verifications

Recently, Kieffer et al. [117,118] have successfully designed fluorine and fluorenyl based derivatives by incorporating electron-withdrawing/donating groups to achieve balanced charge transport. They have obtained highly efficient blue-emitting OLEDs from which the singlet portions have been analyzed to be ranging from 40% to over 60%. These values have been fully justified according to Eq. (19) coupled with quantum chemistry calculations. We can now conclude that in

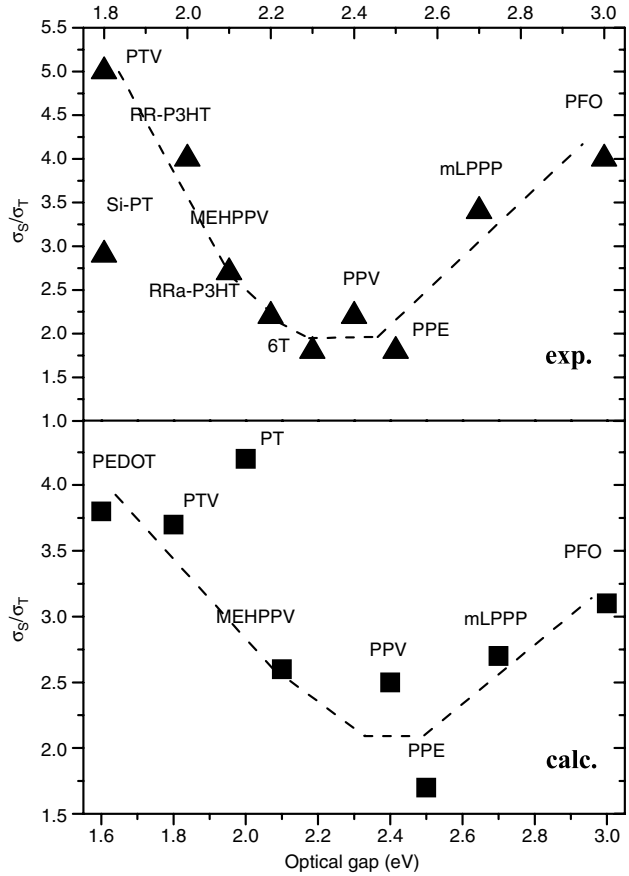

Fig. 6. Comparison between the experimental (exp.) and calculated (calc.) results of the ratios of singlet and triplet exciton formation rates as a function of the optical gaps for different polymers. The dashed lines are guides to the eye.
Source: Reprinted figure with permission from Ref. [109].

the organic electroluminescence, more than 25% singlet exciton can be formed, challenging the conventional wisdom. This is not only supported by photophysical measurements, but also by realization of highly efficient light-emitting materials design. Forrest et al. proposed and succeeded at employing triplet exciton emission through incorporating heavy atoms such as Ir, or Pt to enhance the phosphorescence. Nearly 100% internal quantum efficiency has been attained [28]. However, triplet emission suffers from sharp decreasing of efficiency at high current density due to triplet–triplet annihilation and slow response due to the long triplet life time. Recent advances by Adachi et al. employed thermally activated delayed fluorescence (TADF) is one exciting way to overcome the triplet problem by converting the triplet exciton to singlet [119]. This is done by designing molecules with very small exchange energy. Such an approach can indeed avoid the problem of triplet collision. However, the response time is even longer than triplet emission since one need to wait the triplet reverse intersystem conversion. According to Eq. (19), in order to achieve higher singlet portion from electro-pump, the material design should be directed for large exchange energy Δ_{ST} (in sharp contrast to Adachi's approach) and small singlet exciton binding energy (E_b). It is not easy to achieve both since these have the same origin, the electron correlation. Nevertheless, chemistry can often make magic, especially with the fast developments in both computational technology and theoretical chemistry methodology.

4. Correlation function formalism for optical spectra and photoluminescence efficiency

After electrical excitation and supposing we have excitons, then it comes to the question of photoluminescence. The light-emitting efficiency depends on a competition between radiative decay and non-radiative decay in both singlet manifold (fluorescence) and triplet manifold (phosphorescence). Exciton is a collective excitation of electronic excited state in molecular aggregates or solids with regular intermolecular arrangements. However, in organic light-emitting diodes, the materials are usually in amorphous phase. And the most commonly encountered situation is that the photoluminescence spectrum in solution is very close to that in amorphous films. The exciton state is often approximated by molecular excited state. The excitons in conjugated polymers and molecular aggregates have gained strong interests. Great advances have

been achieved by Spano [120] for molecular crystals, Knoester [121] for nanowires, and Gierschner et al. [122] for polymeric aggregates among others. In these formulations, the exciton–phonon coupling is usually taken as parameter for only one or sometimes two vibration modes with fittings to the optical spectra for understanding the physics origin of optical spectra. Here, we focus on more quantitative descriptions at the polyatomic molecular level by considering all the vibrational modes and their couplings with electronic excited states to work out formalisms ready for quantum chemistry calculations at the first-principles level.

4.1. Interaction of light with molecules

Light is an electromagnetic wave made up of an oscillating electronic field E and an oscillating magnetic field B, which are perpendicular to each other and to the direction of propagation. The quantized electromagnetic field is described as harmonic oscillator $\hat{H} = \sum_{\mathbf{k}\sigma} \hbar\omega_{\mathbf{k}} \left(\hat{n}^{\sigma}_{\mathbf{k}} + \frac{1}{2}\right)$ where σ represents the polarization direction, $\mathbf{k}$ is the corresponding wave vector, which is perpendicular to the unit polarization vector $\hat{\boldsymbol{\eta}}^{\sigma}_{\mathbf{k}}$, $\omega_{\mathbf{k}}$ corresponds to the frequency of wave, and $n^{\sigma}_{\mathbf{k}}$ is the photon number. The vector potential A is given by:

$$\hat{\mathbf{A}}(\mathbf{r}) = \sum_{\mathbf{k}\sigma} \hat{\mathbf{A}}^{\sigma}_{\mathbf{k}}(\mathbf{r}) = \sum_{\mathbf{k}\sigma} \sqrt{\frac{\mathrm{hc}^2}{\omega_{\mathbf{k}} V}} \left(\mathrm{e}^{i\mathbf{k}\cdot\mathbf{r}} \hat{a}^{\sigma}_{\mathbf{k}} + \mathrm{e}^{-i\mathbf{k}\cdot\mathbf{r}} \hat{a}^{\sigma\dagger}_{\mathbf{k}}\right) \hat{\boldsymbol{\eta}}^{\sigma}_{\mathbf{k}} \tag{20}$$

where $a^{\sigma}_{\mathbf{k}}$ and $a^{\sigma\dagger}_{\mathbf{k}}$ denote annihilation and creation bosonic operators; c is the speed of light.

The interacting Hamiltonian between a molecule and the radiation field $\mathbf{A}$ related to the single photon absorption and emission process is expressed as,

$$\hat{H}' = -\sum_{\mathbf{k}\sigma} \sqrt{\frac{\mathrm{h}}{\omega V}} \sum_{j} \left[\frac{q_j}{m_j} \left(\hat{a}^{\sigma}_{\mathbf{k}} + \hat{a}^{\sigma\dagger}_{\mathbf{k}}\right) \left(\hat{\boldsymbol{\eta}}^{\sigma}_{\mathbf{k}} \cdot \mathbf{p}_j\right)\right]. \tag{21}$$

Now, H' as the time-dependent perturbation becomes the physical origin for transition between the different molecular Eigenstates, responsible for both optical absorption and stimulated emission. In case of absorbing one photon, the initial and final states are given by $\left|\Psi^{\mathrm{M}}_i; n^{\sigma}_{\mathbf{k}}, n^{\sigma_\alpha}_{\mathbf{k}_\sigma}, \ldots\right\rangle$, $\left|\Psi^{\mathrm{M}}_f; n^{\sigma}_{\mathbf{k}} - 1, n^{\sigma_\alpha}_{\mathbf{k}_\sigma}, \ldots\right\rangle$, respectively. Then the transition matrix element reads,

$$M^{\sigma}_{\mathbf{k}} = \left\langle \Psi^{\mathrm{M}}_f; n^{\sigma}_{\mathbf{k}} - 1 \left| H' \right| \Psi^{\mathrm{M}}_i; n^{\sigma}_{\mathbf{k}} \right\rangle = -i\sqrt{\frac{2\pi n^{\sigma}\hbar\omega}{V}} \left(\hat{\boldsymbol{\eta}}^{\sigma}_{\mathbf{k}} \cdot \boldsymbol{\mu}_{\mathrm{fi}}\right). \tag{22}$$

Here

$$\boldsymbol{\mu}_{\mathrm{fi}} = \left\langle \Psi^{\mathrm{M}}_f \left| \hat{\boldsymbol{\mu}} \right| \Psi^{\mathrm{M}}_i \right\rangle \tag{23}$$

$$\omega = \left(E^{\mathrm{e}}_f - E^{\mathrm{e}}_i\right)/\hbar. \tag{24}$$

While emitting one photon, the initial and final states becomes $\left|\Psi^{\mathrm{M}}_i; n^{\sigma}_{\mathbf{k}}, n^{\sigma_\alpha}_{\mathbf{k}_\sigma}, \ldots\right\rangle$, $\left|\Psi^{\mathrm{M}}_f; n^{\sigma}_{\mathbf{k}} + 1, n^{\sigma_\alpha}_{\mathbf{k}_\sigma}, \ldots\right\rangle$, respectively, and the transition matrix element is written as

$$M^{\sigma}_{\mathbf{k}} = -i\sqrt{\frac{2\pi\left(n^{\sigma} + 1\right)\hbar\omega}{V}} \left(\hat{\boldsymbol{\eta}}^{\sigma}_{\mathbf{k}} \cdot \boldsymbol{\mu}_{\mathrm{fi}}\right). \tag{25}$$

The transition rate is proportional to

$$\left|M^{\sigma}_{\mathbf{k}}\right|^2 = \begin{cases} \dfrac{2\pi\hbar\omega}{V} \left|\hat{\boldsymbol{\eta}}^{\sigma}_{\mathbf{k}} \cdot \boldsymbol{\mu}_{\mathrm{fi}}\right|^2 n^{\sigma}, & \text{Absorption} \\ \dfrac{2\pi\hbar\omega}{V} \left|\hat{\boldsymbol{\eta}}^{\sigma}_{\mathbf{k}} \cdot \boldsymbol{\mu}_{\mathrm{fi}}\right|^2 \left(n^{\sigma} + 1\right), & \text{Emission.} \end{cases} \tag{26}$$

The number of photons n is related to the amplitude of the electromagnetic field, while $(n + 1)$ is originated from the zero point vibration of the electromagnetic field, which causes the occurrence of spontaneous emission process. Thus for emission, there are contributions from both optical stimulation and spontaneous processes.

4.2. Molecular states and normal mode coordinates

We use a two-level model to describe the electronic states of molecule, namely, the ground state and the excited state, each associated with vibrational states. Under the harmonic approximation, the molecular vibrational state is composed of N ($3n-6$ for nonlinear n atoms molecule or $3n-5$ for linear one) independent harmonic oscillator $\left|\Theta_{iv_i}\right\rangle = \left|\chi_{iv_{i1}}\chi_{iv_{i2}}\cdots\chi_{iv_{iN}}\right\rangle$ and $\left|\Theta_{fv_f}\right\rangle = \left|\chi_{fv_{f1}}\chi_{fv_{f2}}\cdots\chi_{fv_{fN}}\right\rangle$, where v_i and v_f are vibrational quantum numbers and $\left|\chi_{iv_{ik}}\right\rangle$ and $\left|\chi_{fv_{fk}}\right\rangle$ are Eigenstates of

the one-dimensional harmonic oscillator Hamiltonian:

$$\hat{H}_{il} = \frac{1}{2}\left(\hat{P}_{il}^2 + \omega_{il}^2\hat{Q}_{il}^2\right), \tag{27}$$

$$\hat{H}_{fk} = \frac{1}{2}\left(\hat{P}_{fk}^2 + \omega_{fk}^2\hat{Q}_{fk}^2\right). \tag{28}$$

$\hat{P}$ and $\hat{Q}$ are the mass-weighted nuclear normal momentum operator and normal coordinate operator, respectively. The normal mode coordinates Q_{ik} and Q_{fl} can be represented by mass-weighted Cartesian coordinates,

$$Q_{ik} = \sum_{\sigma=1}^{n}\sum_{j=x,y,z} L_{i\sigma j,k}\left(q_{i\sigma j} - q_{i\sigma j}^0\right) \tag{29}$$

$$Q_{fl} = \sum_{\sigma=1}^{n}\sum_{j=x,y,z} L_{f\sigma j,l}\left(q_{f\sigma j} - q_{f\sigma j}^0\right). \tag{30}$$

Here $q_{\sigma j}$ is the mass-reduced Cartesian coordinate of nucleus σ. The superscript 0 in $q_{i\sigma j}^0$ and $q_{f\sigma j}^0$ denotes the equilibrium position of molecular structure in the initial or final electronic state.

Suppose the electronic transition and the subsequent vibrational relaxations do not involve any additional molecular translation or rotation. We put the ground state and excited state molecular geometries in one frame of reference according to the following first (translational) and second (rotational) Eckart conditions,

$$\sum_{\sigma=1}^{n} M_\sigma \mathbf{r}_{i\sigma}^0 = \sum_{\sigma=1}^{n} M_\sigma \mathbf{r}_{f\sigma}^0 = 0 \tag{31}$$

$$\sum_{\sigma=1}^{n} M_\sigma \mathbf{r}_{i\sigma}^0 \times \mathbf{r}_{f\sigma}^0 = 0. \tag{32}$$

Here M_σ is the mass of the σth atom. $\mathbf{r}_{i\sigma}^0$ and $\mathbf{r}_{f\sigma}^0$ are the equilibrium positions of the σ-th atom in the initial and final states, respectively. First, the molecule is translated and rotated to the inertial frame of reference (the equilibrium positions are now labeled as $\mathbf{r}_{i\sigma}'^0$ and $\mathbf{r}_{f\sigma}'^0$) in which the first Eckart condition is automatically satisfied. Second, we set $\mathbf{r}_{f\sigma}^0 = \mathbf{r}_{f\sigma}'^0$, and rotate the initial state geometry, $\mathbf{r}_{i\sigma}^0 = \mathbf{T}\mathbf{r}_{i\sigma}'^0$, to meet the second Eckart condition. The pseudo-rotation matrix T can be calculated according to Ref. [123]. After rearrangement of the two molecular equilibrium structures, the normal coordinates of the two electronic states Q_{ik} and Q_{fl} are related by a Duschinsky rotation matrix $\mathbf{S}_{i\leftarrow f}$ [124] and a coordinate displacement vector $\underline{D}_{i\leftarrow f}$.

$$Q_{ik} = \sum_{l}^{N} S_{i\leftarrow f,kl} Q_{fl} + \underline{D}_{i\leftarrow f,k} \tag{33}$$

where

$$\mathbf{S}_{i\leftarrow f} = \mathbf{L}_i^T \mathbf{L}_f \tag{34}$$

and

$$\underline{D}_{i\leftarrow f} = \mathbf{L}_i^T\left(\mathbf{q}_f^0 - \mathbf{q}_i^0\right). \tag{35}$$

Here $\mathbf{S}_{i\leftarrow f}$ is a unitary matrix, the Duschinsky rotation matrix, whose elements represent the mixing of normal modes in the initial and final electronic states. $\underline{D}_{i\leftarrow f}$ is a displacement vector connecting the minima of the parabolas of the two electronic states. The distortions of the final state PES correspond to the changes of the normal mode frequencies with respect to the initial electronic state within the harmonic oscillator model.

When $\mathbf{S}$ is an identity matrix, Eq. (33) can be simplified as

$$Q_{fk} = Q_{il} + \underline{D}_k. \tag{36}$$

This is the common displaced harmonic oscillator model. In this case, the normal mode frequencies and Eigenvectors are the same for both electronic states except that the equilibrium positions are shifted relative to each other.

4.3. Optical absorption and emission: correlation function formalism

Under the framework of Fermi Golden Rule and Born–Oppenheimer approximation, the absorption cross section, which is defined as the absorption power for unit light intensity, can be expressed as

$$\sigma_{\mathrm{abs}}(\omega, T) = \frac{4\pi^2\omega}{3\hbar c}\sum_{v_i,v_f} P_{iv_i}(T)\left|\left\langle\Theta_{f,v_f}\left|\boldsymbol{\mu}_{\mathrm{fi}}\right|\Theta_{i,v_i}\right\rangle\right|^2 \delta\left(\omega - \omega_{fv_f,iv_i}\right) \tag{37}$$

and the emission spectrum, which is defined as the differential spontaneous photon emission rate, can be written as

$$\sigma_{\rm emi}(\omega,T)=\frac{4\omega^3}{3\hbar c^3}\sum_{v_i,v_f}P_{iv_i}(T)\left|\left\langle\Theta_{f,v_f}\left|\boldsymbol{\mu}_{\rm fi}\right|\Theta_{i,v_i}\right\rangle\right|^2\delta\left(\omega_{iv_i,fv_f}-\omega\right). \tag{38}$$

Here $P_{iv_i}(T)$ is the Boltzmann distribution of the vibration manifolds in the initial electronic state. $\boldsymbol{\mu}^e_{\rm fi}=\left\langle\Phi_f\right|\hat{\mu}\left|\Phi_i\right\rangle$ is the electric transition dipole moment between the two electronic states $\left|\Phi_f\right\rangle$ and $|\Phi_i\rangle$, which is dependent on the molecular vibrational normal coordinate $\mathbf{Q}$,

$$\boldsymbol{\mu}^e_{\rm fi}(\mathbf{Q})=\boldsymbol{\mu}_0+\sum_k\boldsymbol{\mu}_kQ_k+\sum_{k,l}\boldsymbol{\mu}_{kl}Q_kQ_l+O(Q^3). \tag{39}$$

For the strongly dipole-allowed transition, the zero-order term $\boldsymbol{\mu}_0$ is the dominant term. While for the weakly dipole-allowed or dipole-forbidden transitions, the first term is at least to be taken into account, namely, the Herzberg–Teller (HT) effect.

Then, the absorption cross section formula turns into three parts:

$$\sigma_{\rm abs}(\omega,T)=\sigma^{\rm FC}_{\rm abs}(\omega,T)+\sigma^{\rm FC/HT}_{\rm abs}(\omega,T)+\sigma^{\rm HT}_{\rm abs}(\omega,T),$$

where

$$\sigma^{\rm FC}_{\rm abs}(\omega,T)=\frac{4\pi^2\omega}{3\hbar c}\left|\boldsymbol{\mu}_0\right|^2\sum_{v_i,v_f}P_{iv_i}(T)\,\delta\left(\omega-\omega_{fv_f,iv_i}\right)\left|\left\langle\Theta_{f,v_f}\mid\Theta_{i,v_i}\right\rangle\right|^2 \tag{40}$$

$$\sigma^{\rm FC/HT}_{\rm abs}(\omega,T)=\frac{4\pi^2\omega}{3\hbar c}\sum_{v_i,v_f}P_{iv_i}(T)\,\delta\left(\omega-\omega_{fv_f,iv_i}\right)\sum_k\boldsymbol{\mu}_0\cdot\boldsymbol{\mu}_k\left\langle\Theta_{f,v_f}\mid\Theta_{i,v_i}\right\rangle\left\langle\Theta_{i,v_i}\left|Q_k\right|\Theta_{f,v_f}\right\rangle \tag{41}$$

$$\sigma^{\rm HT}_{\rm abs}(\omega,T)=\frac{4\pi^2\omega}{3\hbar c}\sum_{v_i,v_f}P_{iv_i}(T)\,\delta\left(\omega-\omega_{fv_f,iv_i}\right)\sum_{k,l}\boldsymbol{\mu}_k\cdot\boldsymbol{\mu}_l\left\langle\Theta_{f,v_f}\left|Q_k\right|\Theta_{i,v_i}\right\rangle\left\langle\Theta_{i,v_i}\left|Q_l\right|\Theta_{f,v_f}\right\rangle. \tag{42}$$

Fourier transformation for the delta function is,

$$\delta\left(\omega-\omega_{fv_f,iv_i}\right)=\frac{1}{2\pi\hbar}\int_{-\infty}^{\infty}{\rm d}t{\rm e}^{i\left(\omega-\omega_{fv_f,iv_i}\right)t}. \tag{43}$$

Eqs. (40)–(42) can be recast as the following correlation function formalism:

$$\sigma^{\rm FC}_{\rm abs}(\omega,T)=\frac{2\pi\omega}{3\hbar^2c}\left|\boldsymbol{\mu}_0\right|^2\int_{-\infty}^{\infty}{\rm d}t{\rm e}^{i(\omega-\omega_{\rm fi})t}\left[Z_i^{-1}\rho^{\rm FC}_{\rm abs,0}(t,T)\right] \tag{44}$$

$$\sigma^{\rm FC/HT}_{\rm abs}(\omega,T)=\frac{2\pi\omega}{3\hbar^2c}\int_{-\infty}^{\infty}{\rm d}t{\rm e}^{i(\omega-\omega_{\rm fi})t}\left[Z_i^{-1}\sum_k\boldsymbol{\mu}_0\cdot\boldsymbol{\mu}_k\rho^{\rm FC/HT}_{{\rm abs},k}(t,T)\right] \tag{45}$$

$$\sigma^{\rm HT}_{\rm abs}(\omega,T)=\frac{2\pi\omega}{3\hbar^2c}\int_{-\infty}^{\infty}{\rm d}t{\rm e}^{i(\omega-\omega_{\rm fi})t}\left[Z_i^{-1}\sum_{k,l}\boldsymbol{\mu}_k\cdot\boldsymbol{\mu}_l\rho^{\rm HT}_{{\rm abs},kl}(t,T)\right] \tag{46}$$

where Z_i is the partition function, $\tau_i=-i\beta-t/\hbar$, $\tau_f=t/\hbar$, and $\beta=(k_BT)^{-1}$, k_B is the Boltzmann constant. $\hat{H}_i$ and $\hat{H}_f$ represent the multidimensional harmonic oscillator Hamiltonian for the initial and final electronic states, respectively, and the three correlation functions are:

$$\rho^{\rm FC}_{abs,0}(t,T)={\rm Tr}\left[e^{-i\tau_f\hat{H}_f}e^{-i\tau_i\hat{H}_i}\right], \tag{47}$$

$$\rho^{\rm FC/HT}_{abs,k}(t,T)={\rm Tr}\left[Q_{fk}e^{-i\tau_f\hat{H}_f}e^{-i\tau_i\hat{H}_i}\right], \tag{48}$$

and

$$\rho^{\rm HT}_{abs,kl}(t,T)={\rm Tr}\left[Q_{fk}e^{-i\tau_f\hat{H}_f}Q_{fl}e^{-i\tau_i\hat{H}_i}\right]. \tag{49}$$

These can be solved analytically by virtue of multidimensional Gaussian integrations in the path integral framework [37–39],

$$\langle x|\,e^{-i\tau H}\,|\rangle=\sqrt{\frac{a(\tau)}{2\pi i\hbar}}\exp\left\{\frac{i}{\hbar}\left[\frac{1}{2}b(\tau)(x^2+y^2)-a(\tau)xy\right]\right\} \tag{50}$$

to obtain the following solutions:

$$\rho_{abs,0}^{\mathrm{FC}}(t,T)=\sqrt{\frac{\det\left[\mathbf{a}_f\mathbf{a}_i\right]}{\det\left[\mathbf{K}\right]}}\exp\left\{-\frac{i}{\hbar}\left[\frac{1}{2}\underline{F}^T\mathbf{K}\underline{F}-\underline{D}^T\mathbf{E}\underline{D}\right]\right\}, \tag{51}$$

$$\rho_{abs,k}^{\mathrm{FC/HT}}(t,T)=-\rho_{abs,0}^{\mathrm{FC}}(t,T)\left\{\underline{H}_k^{\mathrm{FC/HT}}\mathbf{K}^{-1}\underline{F}\right\}, \tag{52}$$

$$\rho_{abs,kl}^{\mathrm{HT}}(t,T)=\rho_{abs,0}^{\mathrm{FC}}(t,T)\left\{i\hbar\mathrm{Tr}\left[\mathbf{G}_{lk}^{\mathrm{HT}}\mathbf{K}^{-1}\right]+\left(\mathbf{K}^{-1}\underline{F}\right)^T\mathbf{G}_{lk}^{\mathrm{HT}}\left(\mathbf{K}^{-1}\underline{F}\right)\right\}, \tag{53}$$

Here

$$\mathbf{K}=\begin{bmatrix}\mathbf{B} & -\mathbf{A}\\ -\mathbf{A} & \mathbf{B}\end{bmatrix}_{2N\times 2N}$$

$$\underline{F}=\begin{bmatrix}\underline{D}^T\mathbf{E}S & \underline{D}^T\mathbf{E}S\end{bmatrix}_{1\times 2N}^T$$

$$\underline{H}_k^{\mathrm{FC/HT}}=[0_1\cdots 1_k\cdots 0_{2N}]_{1\times 2N}^T$$

$$\mathbf{G}_{kl}^{\mathrm{HT}}=\begin{bmatrix}0_{11} & 0_{12} & \cdots & 0_{1N+l} & \cdots\\ 0_{21} & 0_{22} & \cdots & 0_{2N+l} & \cdots\\ \cdots & \cdots & \cdots & \cdots & \cdots\\ 0_{k1} & 0_{k2} & \cdots & 1_{kN+l} & \cdots\\ \cdots & \cdots & \cdots & \cdots & \cdots\end{bmatrix}_{2N\times 2N}$$

$$\mathbf{A}\equiv\mathbf{a}_f+\mathbf{S}^T\mathbf{a}_i\mathbf{S},$$

$$\mathbf{B}\equiv\mathbf{b}_f+\mathbf{S}^T\mathbf{b}_i\mathbf{S},$$

$$\mathbf{E}\equiv\mathbf{b}_i-\mathbf{a}_i.$$

$\mathbf{a}_{i/f}$ and $\mathbf{b}_{i/f}$ are diagonal with elements

$a_{i/f,k}(\tau_{i/f})=\omega_{i/f,k}/\sin\left(\hbar\omega_{i/f,k}\tau_{i/f}\right)$, and $b_{i/f,k}(\tau_{i/f})=\omega_{i/f,k}/\tan\left(\hbar\omega_{i/f,k}\tau_{i/f}\right)$ respectively.

Defining

$$\tilde{\mu}_{\mathrm{abs}}^2(t,T)=|\vec{\mu}_0|^2-\sum_k\vec{\mu}_0\cdot\vec{\mu}_k\left[\left(\underline{H}_k^{\mathrm{FC/HT}}\right)^T\mathbf{K}^{-1}\underline{F}\right]+\sum_{kl}\vec{\mu}_k\cdot\vec{\mu}_l\left[i\hbar\,\mathrm{Tr}\left[\mathbf{G}_{kl}^{\mathrm{HT}}\mathbf{K}^{-1}\right]+\left(\mathbf{K}^{-1}\underline{F}\right)^T\mathbf{G}_{kl}^{\mathrm{HT}}\left(\mathbf{K}^{-1}\underline{F}\right)\right]. \tag{54}$$

The total absorption spectrum calculation formalism becomes

$$\sigma_{\mathrm{abs}}(\omega)=\frac{2\pi\omega}{3\hbar^2\,\mathrm{c}}\int_{-\infty}^{\infty}\mathrm{d}t\mathrm{e}^{\mathrm{i}(\omega-\omega_{\mathrm{fi}})t}Z_i^{-1}\tilde{\boldsymbol{\mu}}_{\mathrm{abs}}{}^2(t,T)\rho_{\mathrm{abs},0}^{\mathrm{FC}}(t,T). \tag{55}$$

Similarly, the same formalism for the spontaneous emission spectrum is obtained,

$$\sigma_{\mathrm{em}}(\omega)=\frac{2\omega^3}{3\pi\hbar\mathrm{c}^3}\int_{-\infty}^{\infty}\mathrm{d}t\mathrm{e}^{\text{-}\mathrm{i}(\omega-\omega_{\mathrm{if}})t}Z_i^{-1}\tilde{\boldsymbol{\mu}}_{em}{}^2(t,T)\rho_{\mathrm{em},0}^{\mathrm{FC}}(t,T). \tag{56}$$

4.4. Phosphorescence spectrum

Phosphorescence is originated from the spin–orbit coupling, which can be described by the Breit–Pauli operator:

$$\hat{H}^{so}=\frac{e^2\hbar}{2m^2c^2}\left[\sum_i\sum_\sigma Z_\sigma\mathbf{s}_i\cdot\left(\frac{\mathbf{r}_{i\sigma}}{\mathbf{r}_{i\sigma}^3}\times\mathbf{p}_i\right)-\sum_{i\neq j}\left(\frac{\mathbf{r}_{ij}}{\mathbf{r}_{ij}^3}\times\mathbf{p}_i\right)\cdot(\mathbf{s}_i+2\mathbf{s}_j)\right], \tag{57}$$

where Z_σ is the nuclear charges; $\mathbf{r}_{i\sigma}$ and $\mathbf{r}_{ij}$ are the distances between electron i and nucleus σ and electrons i and j respectively; $\mathbf{s}_i$ and $\mathbf{s}_j$are the spin operator for electrons i and j respectively; and $\mathbf{p}_i$ is the momentum operator for electron i.

This coupling term breaks the spin symmetry. In principle, spin is no longer a good quantum number, and is not appropriate to classify the Eigenstates of the Hamiltonian. However, since such coupling is usually weak, we can apply the perturbation theory. The "true" state can still be roughly categorized according to the principal component. Namely, a "singlet (triplet)" state $\left|S'\right\rangle\left(\left|T'\right\rangle\right)$ is expressed as the pure singlet (triplet) state $|S\rangle$ ($|T\rangle$) plus some minor portion of pure singlet (triplet) states:

$$\left|S'\right\rangle=|S\rangle+\sum_n\sum_{\kappa'=1}^{3}\frac{\left\langle{}^3n_{\kappa'}\left|\hat{H}^{\mathrm{SO}}\right|S\right\rangle}{{}^1E_S^0-{}^3E_n^0}\left|{}^3n_{\kappa'}\right\rangle, \tag{58}$$

$$\left|T_k'\right\rangle=|T_k\rangle+\sum_k\frac{\left\langle{}^1k\left|\hat{H}^{\mathrm{SO}}\right|T_\kappa\right\rangle}{{}^3E_T^0-E_\kappa^0}\left|{}^1\kappa\right\rangle. \tag{59}$$

Then the transition dipole moment becomes

$$\boldsymbol{\mu}_{ST_\kappa} = \sum_{k}^{\{\text{singlets}\}} \frac{\langle S|\boldsymbol{\mu}|{}^1k\rangle \left\langle {}^1k \left| \hat{H}^{\text{SO}} \right| T_\kappa \right\rangle}{{}^3E_T^0 - {}^1E_k^0} + \sum_{n}^{\{\text{triplets}\}} \sum_{\kappa'=1}^{3} \frac{\left\langle S \left| \hat{H}^{\text{SO}} \right| {}^3n_{\kappa'} \right\rangle \langle {}^3n_{\kappa'}|\boldsymbol{\mu}|T_\kappa\rangle}{{}^1E_S^0 - {}^3E_n^0}, \tag{60}$$

where κ is the magnetic quantum number, n and k are the intermediate triplet and singlet electronic states, respectively.

Applying the Franck–Condon approximation, the phosphorescence spectrum can be represented as

$$\sigma_{\text{ph}}(\omega, T) = \frac{4\omega^3}{3\hbar c^3} \sum_{v_i, v_f} P_{iv_i}(T) \left| \left\langle \Theta_{f,v_f} \left| \boldsymbol{\mu}_{ST} \right| \Theta_{i,v_i} \right\rangle \right|^2 \delta\left(\omega_{iv_i,fv_f} - \omega\right). \tag{61}$$

4.5. Non-radiative decay rate: combined non-adiabatic and spin–orbit couplings

The molecular excited state can decay radiatively, as described in the previous two sections, but can also decay non-radiatively. Based on the time-dependent second-order perturbation theory and the Born–Oppenheimer adiabatic approximation, the thermal average rate constant from the initial electronic state i with the vibrational quantum numbers v_i to the final electronic state f with the vibrational quantum numbers v_f reads [125]:

$$k_{f\leftarrow i} = \frac{2\pi}{\hbar} \sum_{v_i, v_f} P_{iv_i} \left| H'_{fv_f,iv_i} + \sum_{n,v_n} \frac{H'_{fv_f,nv_n} H'_{nv_n,iv_i}}{E_{iv_i} - E_{nv_n}} \right|^2 \delta\left(E_{iv_i} - E_{fv_f}\right), \tag{62}$$

H' denotes the interaction between two different Born–Oppenheimer states, consisting of two contributions:

$$\hat{H}'\Psi_{iv_i} = \hat{H}^{\text{BO}}\Phi_i(\mathbf{r};\mathbf{Q})\,\Theta_{iv_i}(\mathbf{Q}) + \hat{H}^{\text{SO}}\Phi_i(\mathbf{r};\mathbf{Q})\,\Theta_{iv_i}(\mathbf{Q}) \tag{63}$$

where $\hat{H}^{\text{BO}}$ is the non-adiabatic coupling and $\hat{H}^{\text{SO}}$ is in Eq. (58), and $\mathbf{r}$ and $\mathbf{Q}$ are the electronic and normal mode coordinates, respectively. By neglecting the small term $\partial^2\Phi_i/\partial Q_{fl}^2$, the first term can be expressed as:

$$\left\langle \Phi_f \Theta_{fv_f} \left| \hat{H}^{\text{BO}} \right| \Phi_i \Theta_{iv_i} \right\rangle = -\hbar^2 \sum_k \left\langle \Phi_f \Theta_{fv_f} \left| \frac{\partial \Phi_i}{\partial Q_{fk}} \frac{\partial \Theta_{iv_i}}{\partial Q_{fk}} \right\rangle = \sum_k \left\langle \Phi_f \Theta_{fv_f} \left| \left(\hat{P}_{fk}\Phi_i\right)\left(\hat{P}_{fk}\Theta_{iv_i}\right) \right\rangle \right. \right. \tag{64}$$

k is the index of normal mode; $\hat{P}_{fk}$ is the normal momentum of the kth normal mode in the final electronic state.

We first consider transition between the same spin manifold, internal conversion (IC) from S_1 to S_0 for example. We can ignore the spin–orbit coupling term. According to the Fermi Golden rule, the IC rate can be represented as

$$k_{\text{IC}} = \frac{2\pi}{\hbar} \sum_{v_i, v_f} P_{iv_i}(T) \left| \sum_k \left\langle \Phi_f \left| \hat{P}_k \right| \Phi_i \right\rangle \left\langle \Theta_{fv_f} \left| \hat{P}_k \right| \Theta_{iv_i} \right\rangle \right|^2 \delta\left(E_{iv_i} - E_{fv_f}\right). \tag{65}$$

Applying Fourier transform and Condon approximation, the Eq. (65) is recast as [126]:

$$k_{\text{IC}} = \frac{1}{\hbar^2} \int_{-\infty}^{\infty} \mathrm{d}t\, \mathrm{e}^{i\omega_{\text{if}}t} \sum_{k,l} Z_i^{-1} R_{kl} \rho_{\text{IC},kl}(t, T) \tag{66}$$

where

$$R_{kl} = \left\langle \Phi_f \left| \hat{P}_{fk} \right| \Phi_i \right\rangle \left\langle \Phi_i \left| \hat{P}_{fl} \right| \Phi_f \right\rangle \tag{67}$$

is the non-adiabatic electronic coupling term (the prefactor term). And $\rho_{IC,kl}(t, T)$ is the thermal vibrational correlation function, first obtained by Peng et al. [52]:

$$\rho_{IC,kl}(t, T) = \text{Tr}\left[\hat{P}_{fk} e^{-i\tau_f \hat{H}_f} \hat{P}_{fl} e^{-i\tau_i \hat{H}_i}\right]. \tag{68}$$

We first trace over the initial (excited) state nuclear coordinates:

$$\rho_{IC,kl}(t, T) = \int_{-\infty}^{\infty} d\underline{x}' \left\langle \underline{x}' \right| \hat{P}_{fk} e^{-i\tau_f \hat{H}_f} \hat{P}_{fl} e^{-i\tau_i \hat{H}_i} \left| \underline{x}' \right\rangle \tag{69}$$

where the vector $\underline{x}'$ represents the excited-electronic (initial) state normal mode coordinates Q_{e_j}. Inserting three complete sets of ground (final) states $\underline{y}$, $\underline{z}$ and $\underline{w}$, and one complete set of the initial state $\underline{y}'$:

$$\rho_{IC,kl}(t, T) = \int_{-\infty}^{\infty} dx dy dz dw dx' dy' \left\langle x' \mid x \right\rangle \langle x| \hat{P}_{fk} |y\rangle \langle y| e^{-i\tau_f \hat{H}_f} |z\rangle \langle z| \hat{P}_{fl} |w\rangle \langle w| y'\rangle \left\langle y' \right| e^{-i\tau_i \hat{H}_i} \left| x' \right\rangle. \tag{70}$$

The transformation between two spaces is the Duschinsky rotation:

$$\left\langle \underline{x}' \mid \underline{x} \right\rangle = \delta[\underline{x}' - (S\underline{x} + \underline{D})]. \tag{71}$$

And the normal momentum matrix element is:

$$\langle x_k | \hat{P}_{fk} | y_k \rangle = -ih\frac{\partial}{\partial x_k}\delta(x_k - y_k). \tag{72}$$

Along with Eq. (50), we can get the following analytical solution:

$$\rho_{IC,kl}(t,T) = \sqrt{\frac{\det\left[\mathbf{a}_f\mathbf{a}_i\right]}{\det[\mathbf{K}]}}\exp\left\{-\frac{i}{\hbar}\left[\frac{1}{2}\underline{F}^T\mathbf{K}^{-1}\underline{F} - \underline{D}^T\mathbf{E}\underline{D}\right]\right\} \times \left\{i\hbar\mathrm{Tr}\left[\mathbf{G}_{lk}^{\mathrm{IC}}\mathbf{K}^{-1}\right] + \left(\mathbf{K}^{-1}\underline{F}\right)^T\mathbf{G}_{lk}^{\mathrm{IC}}\left(\mathbf{K}^{-1}\underline{F}\right) - \underline{H}_{kl}^{\mathrm{IC}}\mathbf{K}^{-1}\underline{F}\right\}. \tag{73}$$

The definitions of matrices $\mathbf{G}$, $\mathbf{K}$, and vectors $\underline{F}$, $\underline{H}$, have been given in previous sections and in Ref. [126].

Now, we look at the non-radiative decay between difference spin states, from T_1 to S_0 for example. Expanding Eq. (62), we obtain

$$k_{f\leftarrow i} = k_{f\leftarrow i}^{(0)} + k_{f\leftarrow i}^{(1)} + k_{f\leftarrow i}^{(2)} \tag{74}$$

where

$$k_{f\leftarrow i}^{(0)} = \frac{2\pi}{\hbar}\sum_{v_i,v_f}P_{iv_i}\left|H'_{fv_f,iv_i}\right|^2\delta\left(E_{iv_i} - E_{fv_f}\right), \tag{75}$$

$$k_{f\leftarrow i}^{(1)} = \frac{2\pi}{\hbar}\sum_{v_i,v_f}P_{iv_i}\cdot 2Re\left(H'_{fv_f,iv_i}\sum_{n,v_n}\frac{H'_{iv_i,nv_n}H'_{nv_n,fv_f}}{E_{iv_i} - E_{nv_n}}\right)\delta\left(E_{iv_i} - E_{fv_f}\right), \tag{76}$$

$$k_{f\leftarrow i}^{(2)} = \frac{2\pi}{\hbar}\sum_{v_i,v_f}P_{iv_i}\left|\sum_{n,v_n}\frac{H'_{fv_f,nv_n}H'_{nv_n,iv_i}}{E_{iv_i} - E_{nv_n}}\right|^2\delta\left(E_{iv_i} - E_{fv_f}\right). \tag{77}$$

For the zeroth order, $k_{f\leftarrow i}^{(0)}$, $\hat{H}^{\mathrm{BO}}$ term in Eq. (63) does not make any contribution because of the spin symmetry. So we have

$$k_{f\leftarrow i}^{(0)} = \frac{2\pi}{\hbar}\sum_{v_i,v_f}P_{iv_i}\left|\left\langle\Phi_f\Theta_{fv_f}\left|\hat{H}^{\mathrm{SO}}\right|\Phi_i\Theta_{iv_i}\right\rangle\right|^2\delta\left(E_{iv_i} - E_{fv_f}\right). \tag{78}$$

Applying the Condon approximation, Eq. (78) can be deduced to

$$k_{f\leftarrow i}^{(0)} = \frac{2\pi}{\hbar}R_{\mathrm{fi}}^{\mathrm{isc}}Z_i^{-1}\sum_{v_i,v_f}\mathrm{e}^{-\beta E_{iv_i}}\left|\left\langle\Theta_{fv_f} \mid \Theta_{iv_i}\right\rangle\right|^2\delta\left(E_{iv_i} - E_{fv_f}\right) \tag{79}$$

where

$$R_{\mathrm{fi}}^{\mathrm{isc}} \equiv \left|H_{\mathrm{fi}}^{\mathrm{SO}}\right|^2 \equiv \left|\left\langle\Phi_f\left|\hat{H}^{\mathrm{SO}}\right|\Phi_i\right\rangle\right|^2. \tag{80}$$

For the second term $k_{f\leftarrow i}^{(1)}$, we must simultaneously consider the contributions from both terms $\hat{H}^{\mathrm{BO}}$, $\hat{H}^{\mathrm{SO}}$ and their cross product term. Using Condon approximation, neglecting the second order of $H_{in}^{\mathrm{SO}}H_{nf}^{\mathrm{SO}}$ term, we obtain

$$H'_{fv_f,iv_i} = H_{\mathrm{fi}}^{\mathrm{SO}}\left\langle\Theta_{fv_f} \mid \Theta_{iv_i}\right\rangle, \tag{81}$$

$$\sum_{n,v_n}\frac{H'_{iv_i,nv_n}H'_{nv_n,fv_f}}{E_{iv_i} - E_{nv_n}} = \sum_{n,v_n,k}\frac{\left\langle\Theta_{iv_i}\left|\hat{H}_{in}^{\mathrm{SO}}\right|\Theta_{nv_n}\right\rangle\left\langle\Theta_{nv_n}\left|\left\langle\Phi_n \mid \hat{P}_{fk}\Phi_f\right\rangle\hat{P}_{fk}\right|\Theta_{fv_f}\right\rangle}{E_{iv_i} - E_{n\mu}} + \sum_{n,v_n,k}\frac{\left\langle\Theta_{iv_i}\left|\left\langle\Phi_i \mid \hat{P}_{fk}\Phi_n\right\rangle\hat{P}_{fk}\right|\Theta_{nv_n}\right\rangle\left\langle\Theta_{nv_n}\left|\hat{H}_{nf}^{\mathrm{SO}}\right|\Theta_{fv_f}\right\rangle}{E_{iv_i} - E_{nv_n}}. \tag{82}$$

Further applying Placzek approximation, $E_{iv_i} - E_{nv_n} \approx E_i - E_n$, Eq. (82) can be recast into

$$\sum_{n,v_n}\frac{H'_{iv_i,nv_n}H'_{nv_n,fv_f}}{E_{iv_i} - E_{nv_n}} = \sum_k T_{\mathrm{if},k}\left\langle\Theta_{iv_i}\left|\hat{P}_{fk}\right|\Theta_{fv_f}\right\rangle, \tag{83}$$

where

$$T_{\mathrm{if},k} \equiv \sum_n \left(H_{in}^{\mathrm{SO}} \frac{\left\langle \Phi_n \left| \hat{P}_{fk} \right| \Phi_f \right\rangle}{E_i - E_n} + \frac{\left\langle \Phi_i \left| \hat{P}_{fk} \right| \Phi_n \right\rangle}{E_i - E_n} H_{nf}^{\mathrm{SO}} \right). \tag{84}$$

Merging Eqs. (81) and (83), we have

$$k_{f\leftarrow i}^{(1)} = Re\left[\sum_k \frac{2\pi}{\hbar} 2R_{\mathrm{fi},k}^{\mathrm{isc}} Z_i^{-1} \sum_{v_i,v_f} \mathrm{e}^{-\beta E_{iv_i}} P_{fv_f,iv_i,k}^{(1)} \delta\left(E_{iv_i} - E_{fv_f}\right) \right]. \tag{85}$$

Here

$$R_{\mathrm{fi},k}^{\mathrm{isc}} \equiv H_{\mathrm{fi}}^{\mathrm{SO}} T_{\mathrm{if},k},$$

and

$$P_{fv_f,iv_i,k}^{(1)} \equiv \left\langle \Theta_{iv_i} \left| \hat{P}_{fk} \right| \Theta_{fv_f} \right\rangle \left\langle \Theta_{fv_f} \mid \Theta_{iv_i} \right\rangle.$$

Similarly, the third term can be recast as the following

$$k_{f\leftarrow i}^{(2)} = \sum_{k,l} \frac{2\pi}{\hbar} R_{\mathrm{fi},kl}^{\mathrm{isc}} Z_i^{-1} \sum_{v_i,v_f} \mathrm{e}^{-\beta E_{iv_i}} P_{fv_f,iv_i,kl}^{(2)} \delta\left(E_{iv_i} - E_{fv_f}\right). \tag{86}$$

Here

$$R_{\mathrm{fi},kl}^{\mathrm{isc}} \equiv T_{\mathrm{if},k} T_{\mathrm{fi},l},$$

and

$$P_{fv_f,iv_i,kl}^{(2)} = \left\langle \Theta_{iv_i} \left| \hat{P}_{fk} \right| \Theta_{fv_f} \right\rangle \left\langle \Theta_{fv_f} \left| \hat{P}_{fl} \right| \Theta_{iv_i} \right\rangle.$$

Following the same procedure outlined previously, we can write down the vibration correlation functions:

$$\begin{aligned} k_{f\leftarrow i}^{(0)} &= \frac{1}{\hbar} R_{\mathrm{fi}}^{\mathrm{isc}} \int_{-\infty}^{\infty} \mathrm{d}\tau \mathrm{e}^{iE_{\mathrm{if}}\tau} Z_i^{-1} \sum_{v_i,v_f} \left\langle \Theta_{iv_i} \left| \mathrm{e}^{-i\tau E_{fv_f}} \right| \Theta_{fv_f} \right\rangle \left\langle \Theta_{fv_f} \left| \mathrm{e}^{-i(-\tau - i\beta)E_v^i} \right| \Theta_{iv_i} \right\rangle \\ &\equiv \frac{1}{\hbar^2} R_{\mathrm{fi}}^{\mathrm{isc}} \int_{-\infty}^{\infty} \mathrm{d}t \mathrm{e}^{i\omega_{\mathrm{if}}t} Z_i^{-1} \rho_{\mathrm{fi}}^{(0)}(t,T), \end{aligned} \tag{87}$$

$$\begin{aligned} k_{f\leftarrow i}^{(1)} &= Re\left[\frac{1}{\hbar^2} \int_{-\infty}^{\infty} \mathrm{d}t \mathrm{e}^{i\omega_{\mathrm{if}}t} Z_i^{-1} \sum_{v_i,v_f,k} 2R_{\mathrm{fi},k}^{\mathrm{isc}} \left\langle \Theta_{iv_i} \left| \hat{P}_{fk} \mathrm{e}^{-i\tau E_u^f} \right| \Theta_{fv_f} \right\rangle \left\langle \Theta_{fv_f} \left| \mathrm{e}^{-i(-\tau - i\beta)E_{iv_i}} \right| \Theta_{iv_i} \right\rangle \right] \\ &\equiv Re\left[\frac{1}{\hbar^2} \int_{-\infty}^{\infty} \mathrm{d}t \mathrm{e}^{i\omega_{\mathrm{if}}t} Z_i^{-1} \sum_k 2R_{\mathrm{fi},k}^{\mathrm{isc}} \rho_{\mathrm{fi},k}^{(1)}(t,T) \right] \end{aligned} \tag{88}$$

$$\begin{aligned} k_{f\leftarrow i}^{(2)} &= \frac{1}{\hbar^2} \int_{-\infty}^{\infty} \mathrm{d}t \mathrm{e}^{i\omega_{\mathrm{if}}t} Z_i^{-1} \sum_{v_i,v_f,k,l} R_{\mathrm{fi},kl}^{\mathrm{isc}} \left\langle \Theta_{iv_i} \left| \hat{P}_{fk} \mathrm{e}^{-i\tau E_{fv_f}} \right| \Theta_{fv_f} \right\rangle \left\langle \Theta_{fv_f} \left| \hat{P}_{fl} \mathrm{e}^{-i(-\tau - i\beta)E_{iv_i}} \right| \Theta_{iv_i} \right\rangle \\ &\equiv \frac{1}{\hbar^2} \int_{-\infty}^{\infty} \mathrm{d}t \mathrm{e}^{i\omega_{\mathrm{if}}t} Z_i^{-1} \sum_{k,l} R_{\mathrm{fi},kl}^{\mathrm{isc}} \rho_{\mathrm{fi},kl}^{(2)}(t,T). \end{aligned} \tag{89}$$

It is noted immediately that $\rho^{(0)}$ is simply the Franck–Condon factor Eq. (51) and $\rho^{(2)}$ is Eq. (73). $\rho^{(1)}$ can be solved similarly:

$$\begin{aligned} \rho_{\mathrm{fi},k}^{(1)}(t,T) &\equiv \mathrm{Tr}\left[\hat{P}_{fk} \mathrm{e}^{-i\tau_f \hat{H}_f} \mathrm{e}^{-i\tau_i \hat{H}_i} \right] \\ &= \int \mathrm{d}\underline{x} \left\langle \underline{x} \left| \hat{P}_{fk} \mathrm{e}^{-i\tau_f \hat{H}_f} \mathrm{e}^{-i\tau_i \hat{H}_i} \right| \underline{x} \right\rangle \\ &= \int \mathrm{d}\underline{x}\mathrm{d}\underline{y}\mathrm{d}\underline{z}\mathrm{d}\underline{m}'\mathrm{d}\underline{n}' \left\langle \underline{x} \left| \hat{P}_{fk} \right| \underline{y} \right\rangle \left\langle \underline{y} \left| \mathrm{e}^{-i\tau_f \hat{H}_f} \right| \underline{z} \right\rangle \left\langle \underline{z} \mid \underline{m}' \right\rangle \left\langle \underline{m}' \left| \mathrm{e}^{-i\tau_i \hat{H}_i} \right| \underline{n}' \right\rangle \left\langle \underline{n}' \mid \underline{x} \right\rangle \\ &= \int \mathrm{d}\underline{x}\mathrm{d}\underline{y}\mathrm{d}\underline{z}\mathrm{d}\underline{m}'\mathrm{d}\underline{n}' - i\hbar\delta'(x_k - y_k) \prod_{j(\neq k)} \delta\left(x_j - y_j\right) \\ &\quad \sqrt{\frac{\det[\mathbf{a}_f]}{(2\pi i\hbar)^N}} \exp\left\{ \frac{i}{\hbar} \left[\frac{1}{2} \left(\underline{y}^T \mathbf{b}_f \underline{y} + \underline{z}^T \mathbf{b}_f \underline{z} \right) - \underline{y}^T \mathbf{a}_f \underline{z} \right] \right\} \end{aligned}$$

$$\delta\left(\underline{z}-\underline{m}'\right)$$
$$\sqrt{\frac{\det[\mathbf{a}_i]}{(2\pi i\hbar)^N}}\exp\left\{\frac{i}{\hbar}\left[\frac{1}{2}\left(\underline{m}'^T\mathbf{b}_i\underline{m}'+\underline{n}'^T\mathbf{b}_i\underline{n}\right)-\underline{m}'^T\mathbf{a}_i\underline{n}'\right]\right\}$$
$$\delta\left(\underline{n}'-\underline{x}\right)$$
$$=-\underline{H}_k^T\mathbf{K}^{-1}\underline{F}\sqrt{\frac{\det\left[\mathbf{a}_f\mathbf{a}_i\right]}{\det\left[\mathbf{K}\right]}}\exp\left\{\frac{i}{\hbar}\left[-\frac{1}{2}\underline{F}^TK^{-1}\underline{F}+\underline{D}^TE\underline{D}\right]\right\}. \tag{90}$$

The prefactor for the non-adiabatic electronic coupling can be written under the first-order perturbation theory as [125]:

$$\left\langle\Phi_f\mid\frac{\partial\Phi_i}{\partial Q_{fk}}\right\rangle\approx\frac{\left\langle\Phi_f^0\left|\frac{\partial V}{\partial Q_{fk}}\right|\Phi_i^0\right\rangle}{E\left(\Phi_i^0\right)-E\left(\Phi_f^0\right)}. \tag{91}$$

Using the following relations,

$$L_{f\sigma j,k}=\frac{\partial q_{\sigma j}}{\partial Q_{fk}}, \tag{92}$$

$$q_{\sigma j}=\sqrt{M_\sigma}R_{\sigma j}, \tag{93}$$

$R_{\sigma j}$ is the Cartesian coordinate of the σth atom along the jth direction. The coupling term is recast as

$$\left\langle\Phi_f^0\left|\frac{\partial V}{\partial Q_{fk}}\right|\Phi_i^0\right\rangle=-\sum_\sigma\frac{Z_\sigma e^2}{\sqrt{M_\sigma}}\sum_{j=x,y,z}E_{f\leftarrow i,\sigma j}L_{\sigma j}. \tag{94}$$

The transition electric field $E_{f\leftarrow i,\sigma\tau}=\int d\mathbf{r}\rho_{fi}(\mathbf{r})\frac{e\left(r_j-R_{\sigma j}\right)}{|\mathbf{r}-R_{\sigma}|^3}$ was computed at the TDDFT level using Gaussian 09 program.

Alternatively, Eq. (91) can be written as,

$$\frac{\left\langle\Phi_f^0\left|\frac{\partial V}{\partial Q_{fk}}\right|\Phi_i^0\right\rangle}{E\left(\Phi_i^0\right)-E\left(\Phi_f^0\right)}=\sum_\sigma^{\{\text{nuclei}\}}\sum_j^{x,y,z}M_\sigma^{-\frac{1}{2}}\tau_{f\leftarrow i,\sigma j}L_{f\sigma j,k}. \tag{95}$$

Here $\tau_{f\leftarrow i,\sigma j}\equiv\left\langle\Phi_f^0\left|\frac{\partial V}{\partial R_{\sigma j}}\right|\Phi_i^0\right\rangle/\left(E\left(\Phi_i^0\right)-E\left(\Phi_f^0\right)\right)$ can be calculated at CASSCF level in MOLPRO program [127] for small molecule with high precision and Turbomole [128] under TDDFT framework.

4.6. Computational study of photophysics for polyatomic molecules and aggregation induced emission phenomena

4.6.1. Combined computational methodologies

With all the formalisms at hand, now we are ready to investigate the photophysics for molecules and aggregates with inputs from quantum chemistry calculations. The electronic structure information, including geometry optimization, vibrational modes for the electronic ground and excited states were carried out using the common quantum chemical software, such as Gaussian 09 [129], Turbomole or QCHEM [130] programs. For the relatively large molecules, the ground-state electronic structures were obtained at the level of density functional theory (DFT); the excited-state was calculated at the level of time-dependent DFT (TDDFT). The hybrid functional B3LYP, PBE0 and the range-separated hybrid functional CAM-B3LYP (depending on the actual molecules) were usually adopted with the basis set 6-31G* or PVTZ except Lan2DZ or SDD for the transition metals. During the geometry optimizations, the energy convergence thresholds for the electronic ground and excited states were usually set to be 10^{-7} and 10^{-8} atomic unit, respectively.

For the molecular aggregates, we combine quantum mechanics with molecular mechanics (QM/MM). Here as a first step, we ignore both the intermolecular charge transfer and excitonic effects. The intermolecular interaction is taken only at the electrostatic potential level. In QM/MM calculation, the whole system is separated into two parts, a QM region with chemical interests (with excited states) and an MM region as the surrounding environments. In our computational model, one central molecule was chosen for QM calculation and the surrounding two layers molecules as cut from crystal structures were dealt with MM method.

The QM/MM calculations were carried out using the ChemShell 3.4 interface package [131]. The geometry optimization is carried out by using the hybrid delocalized internal coordinate (HDLC) optimizer [132], with QM molecule active and MM molecules frozen. Turbomole 6.3 and DL-POLY program package [133] were used to calculate the energies and gradients of the QM and MM molecules, respectively. All the electronic structure QM calculations were done using the same methods mentioned above for the isolated molecules. The MM part is treated with the General Amber Force Field (GAFF) [134], and the QM/MM interactions were treated using the electrostatic embedding scheme [135].

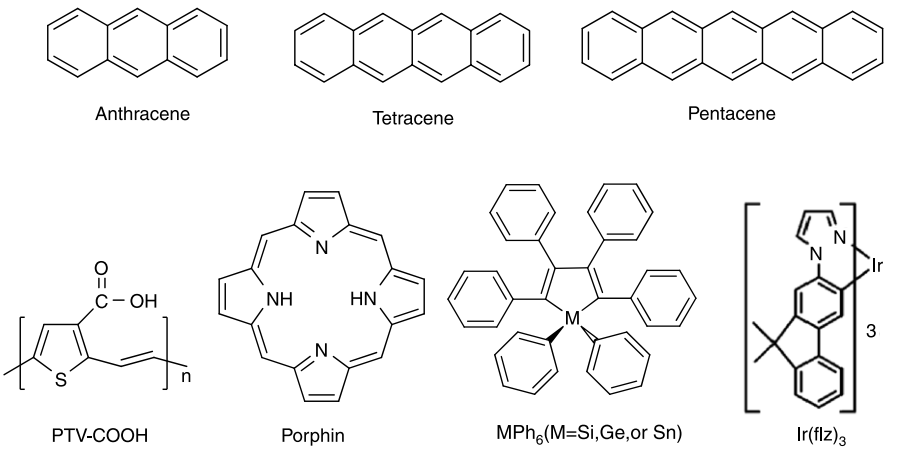

Fig. 7. Molecular structures of the chromophores.

4.6.2. Optical emission and absorption spectra

Emission (fluorescence or phosphorescence) spectrum is essential for the color of OLED display device, in addition to providing information on dynamics of ultrafast phenomena and/or the structure parameters. We firstly compared the calculated optical spectra with the experiments for a variety of systems (Fig. 7) to validate our formulae introduced previously.

Anthracene, tetracene, and pentacene are chosen as benchmark systems because their photophysical properties have been well-established and they are typical organic semiconductors [136–141]. Fig. 8 compares the calculated absorption and fluorescence spectra including HT term and the available experiments at different temperatures, as well as the previous calculations in anthracene, tetracene and pentacene. Here, the theoretical and experimental spectra are all normalized and the 0–0 transition energies $\hbar\omega_{00}$ are set as the origin. It is seen that the FC term dominates the entire line shapes for both absorption and emission spectra. The absorption and emission spectra in anthracene and tetracene are well reproduced by our calculations without invoking any broadening factor. Especially the hot bands observed in the measurements are reproduced here, which have been absent in the simple sum-over-states formalism derived at $T = 0$ K [139]. For pentacene, in order to eliminate the oscillation feature of the correlation function at low temperature, a Lorentzian broadening of 30 cm^{-1} is introduced in the time integration Eqs. (55) and (56). Fig. 8(e) depicts a peak 1556 cm^{-1} stemming from the HT term, which was missing in previous calculation [139]. The experimental spectra including features with small intensity are nicely reproduced by our formalism.

The electronic structure and spectra of free-base porphyrin (H_2P) has been extensively investigated due to its importance in biological sciences [142–145]. The dark Q band was discovered in the visible region, with weakly dipole-allowed transition between the ground and the first excited state. It is expected that the Herzberg–Teller effect is essential since the Franck–Condon term is small. We depict both the FC and FCHT spectra in Fig. 9 at 300 K. It is seen that the FC spectra are very narrow with vanishingly small intensity around the 0–0 transition; while the FCHT spectra are both broad and intensive, at a position far away from the 0–0 transition, in good agreement with the previous results [142].

Organo-metallic molecules can emit light from both singlet and triplet excited states thus with 100% internal quantum luminescence efficiency [26,27]. So far, the organo-transition metal complexes have been the focus in many industrial and academic researches. In particular, cyclometalated iridium complexes with emission colors that vary from blue to red have received great attentions [146,147]. *fac*-Ir$(flz)_3$ (flz=1-[(9,9-dimethyl-2-fluorenyl)]pyrazoyl) is one of the most commonly investigated phosphorescence molecules [148,149]. We employed Eqs. (60) and (61) to calculate its phosphorescence spectrum at 77 K at the level of CAM-B3LYP/6-31G** which is plotted in Fig. 10. The experimental data is also shown there for comparison with a 0.029 eV red-shift in order to match the 0–0 transition. Not only the main peak but also the well-defined vibronic fine structures reproduce well the experimental spectrum.

4.6.3. Theoretical design of photovoltaic polymers based on thienylene vinylene

In a bulk heterojunction polymer solar cell, light is harvested by semiconducting polymer as donor and a subsequent charge transfer occurs at the polymer interface with acceptor (typically fullerene derivatives). In one hand, polymer should possess small band gap to harvest as much as possible solar emission. In another hand, polymer should be slightly emissive to help exciton migration: since exciton diffusion is proportional to the overlap between emission and absorption. Poly(2,5-thienylene vinylene) (PTV) derivatives have been considered as the promising candidates as donor materials due to the low band gap 1.55∼1.8 eV [151–154]. However, the pristine PTV does not show any appreciable photovoltaic property. This is due to the fact that lowest excited state in PTV is of $2A_g$ symmetry which does not allow any appreciable optical emission thus prohibiting energy transfer and the subsequent charge separation. Following the strategy outlined in Section 2.4, we

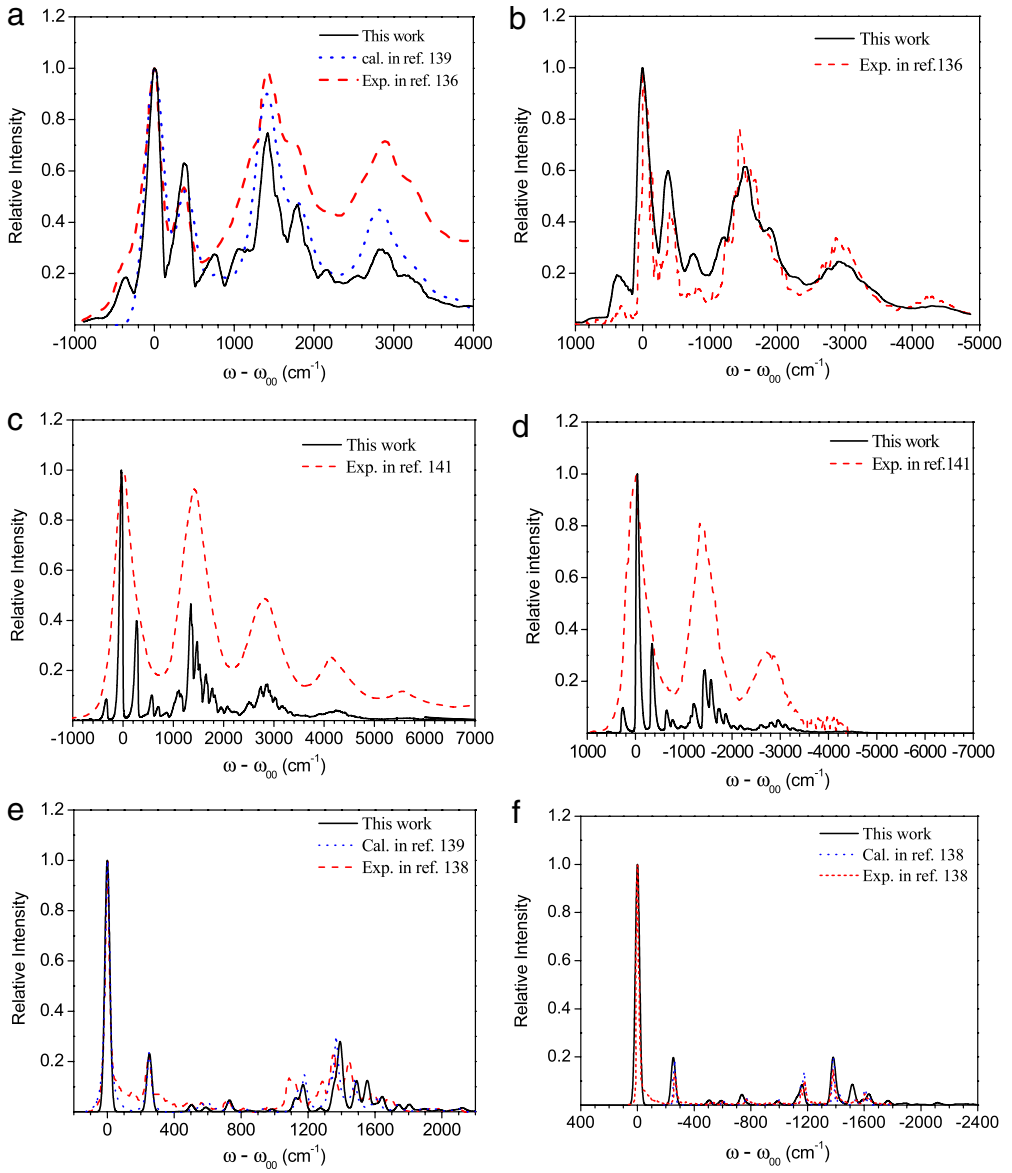

Fig. 8. Comparison of our results (solid) with the experimental ones (dashed) and with previous theoretical results (dotted): (a) absorption spectrum at 423 K for anthracene; (b) emission spectrum at 433 K for anthracene; (c) and (d) are the absorption and emission spectra at 300 K for tetracene respectively; (e) and (f) are the absorption and emission spectra at 5 K for pentacene respectively.
Source: Reprinted figure with permission from Ref. [39].

investigate the chemical substitution effects on both the lowest-lying excited state ordering. It is found that for R = COOH, NO_2 and CHO (chemical structures see Fig. 11), the lowest excited state becomes $1B_u$, while for R = CH_3 or OH, there is no excited state alteration [150]. Then we calculate the absorption and emission spectra for the experimentally available PTV-COOH at 300 K, shown in Fig. 12, in comparison with the experiment. Oligo(thienylene vinylene) (OTV) including six unit cells were chosen as the computational model in the spectrum calculation. It is clearly seen that the line shapes and stokes shift in theoretical spectra are in excellent agreement with the experimental results, which again validates our vibration correlation formalism. To demonstrate the advantage of such formalism, we compare the computer wall time for the emission spectrum as a function of the number of normal modes for the series of nTV-COOH (n = 2–6), and plotted them in Fig. 13. As the number of normal modes N increases, the computation time grows as N^3, namely, matrix manipulation. In our formalism, all the vibrational quantum numbers (from 0 to ∞) for all the modes are automatically included. In contrast, for the traditional sum-over-states approach, one needs a cutoff for vibrational quanta. For example, considering the simplest 0 K case, the computational timescale is $(a + 1)^N$, where a is a cutoff of vibrational quanta. The inset of Fig. 13 shows the computing

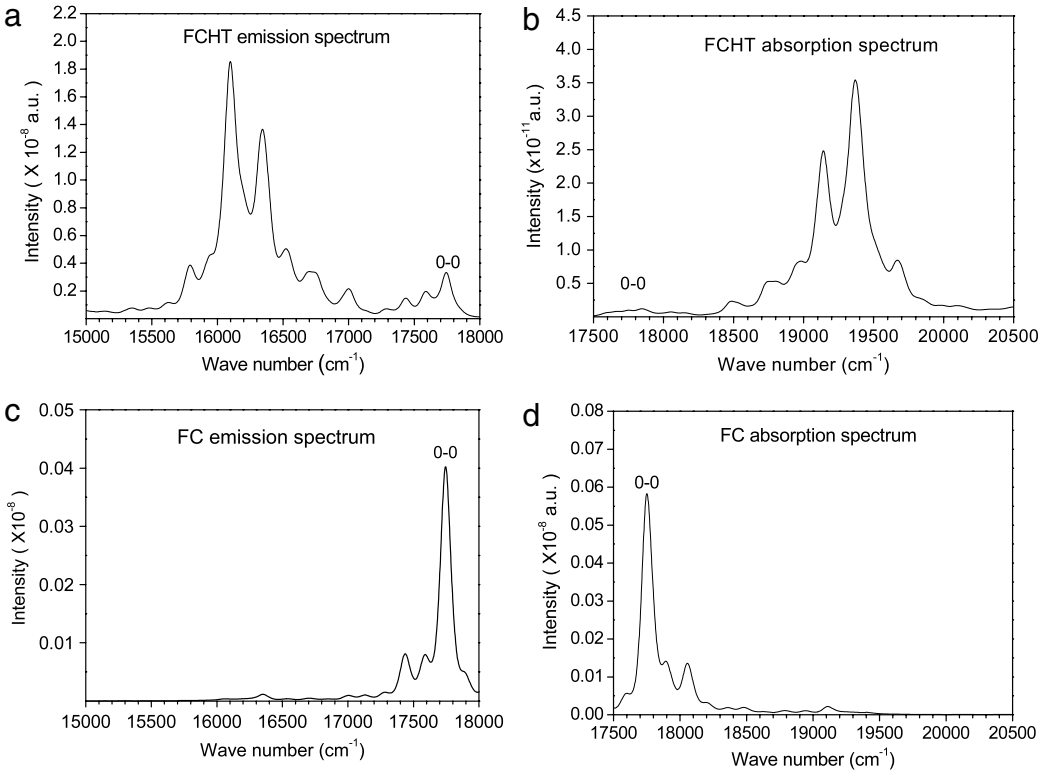

Fig. 9. Theoretical emission (left) and absorption (right) spectra of H_2P at 300 K: (a) and (b) with both FC and HT contributions; (c) and (d) with FC contribution only.
Source: Reprinted figure with permission from Ref. [39].

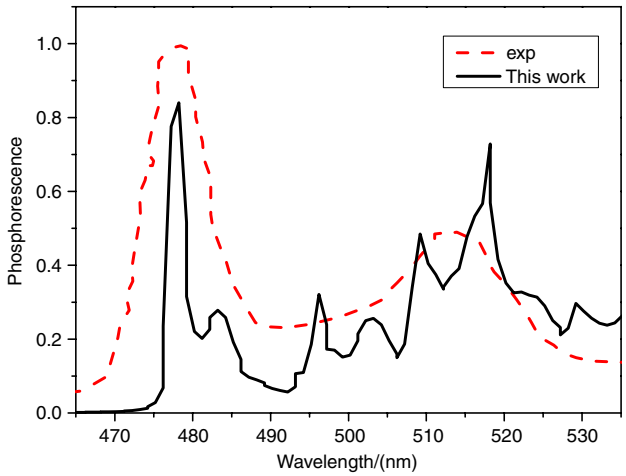

Fig. 10. Comparison of the calculated phosphorescent spectra with the experiment for *fac*-Ir(flz)$_3$ at 77 K.

times versus the number of selected "important" modes (with substantial Huang–Rhys factor) for 6TV-COOH consisting of 240 normal modes, where a is set to 2, i.e. $v = 0, 1$. The curve grows exponentially with increasing N. For example of 6TV-COOH, out of 240 normal modes, one chooses only 24 "important" modes and the calculation costs almost 1000 min.

Experimentally, the COOH substituted PTV indeed demonstrated photovoltaic effect (about 2% power conversion efficiency) [154]. In Fig. 14, we compare the absorption and emission spectra for the three substituted PTV derivatives.

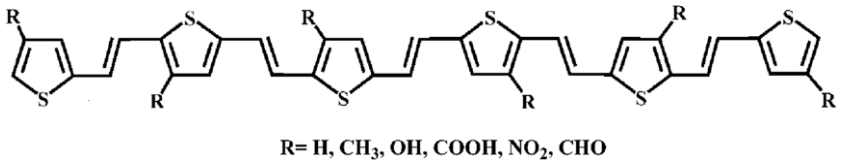

Fig. 11. Oligomer structures of pristine and substituted polythienylene vinylene.
Source: Reprinted figure with permission from Ref. [150].

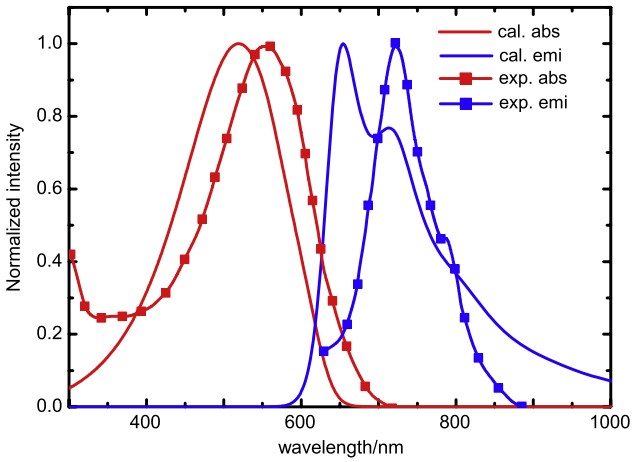

Fig. 12. Comparison of optical absorption and emission spectra between theory ($T = 300$ K) and experiment (in dilute CHCl3 solution) for PTV-COOH.
Source: Reprinted figure with permission from Ref. [150].

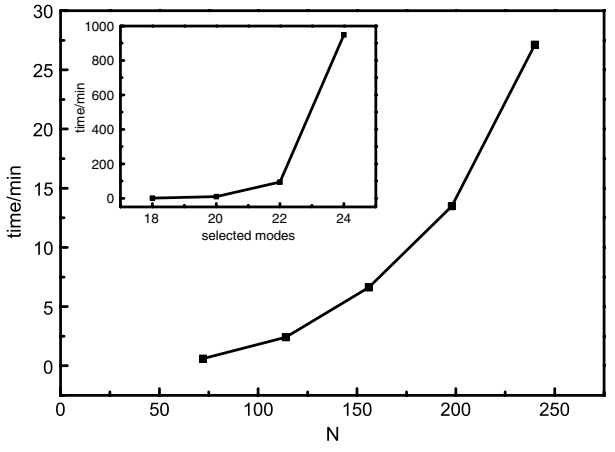

Fig. 13. Computing time of emission rate versus the number of normal modes (N) for nTV-COOH ($n = 2 \sim 6$) by our method. The traditional method keeping only 2 quanta is shown in the inset.
Source: Reprinted figure with permission from Ref. [150].

It is found that CHO substitution possesses the maximum spectral overlap, favoring energy transfer. In addition, CHO-PTV also has the longest excited state life time, thus long exciton diffusion length.

4.6.4. From excited-state decay to aggregation induced emission

In this part of the Report, we focus on the excited state decay rates, radiative and non-radiative. The radiative decay rate is simply the full integration of emission spectrum, $k_r = \int d\omega \sigma_{emi}(\omega)$. The non-radiative decay has been discussed in

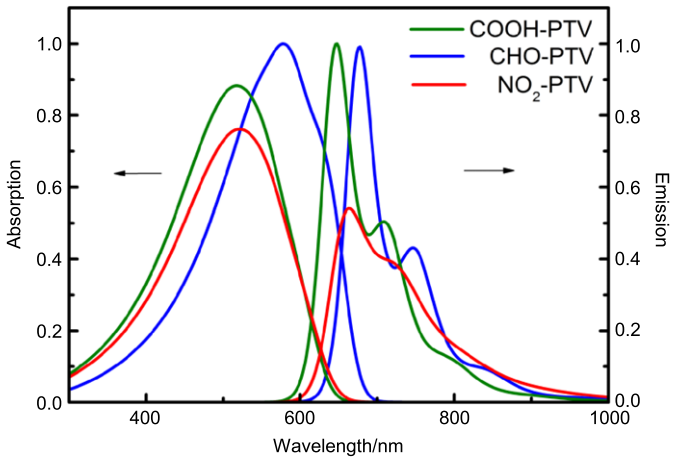

Fig. 14. Theoretical optical spectra for PTV derivatives.
Source: Reprinted figure with permission from Ref. [150].
© 2012, Royal Society of Chemistry

Section 4.5. In particular, our primary interest is on the exotic aggregation induced emission (AIE) phenomena. It has been long established that molecular aggregate tends to suppress luminescence, because of (i) intermolecular charge transfer which lowers the chance of charge recombination; (ii) intermolecular energy transfer which often traps the exciton in a quenching site or in site with reduced efficiency; (iii) Davidov splitting which makes the lower energy state component with reduced oscillator strength. This is called Aggregation Caused Quenching (ACQ) phenomena, bad for OLEDs: the device works in solid state. Tang and co-workers discovered the AIE phenomena [155]. It has continuously been the focus of intensive research [156–158]. The design and synthesis of new AIE luminogens have led to a variety of novel AIE molecules including Group 14 metalloles (siloles, germoles, and stannoles), tetraphenylethenes, dibenzofulvene, diaminobenzene-cored derivatives, triarylamine, distyrylanthracene, polymeric derivatives and many others [159]. The discovery of AIE-active molecules opens a new way to improve the performance of the optoelectronic devices.

It is desirable to understand the mechanism of such exotic photochemistry phenomenon. Several possible AIE mechanics have been proposed, including the restriction of intramolecular rotations [160,161], *J*-aggregation formation [162,163], excimer formation [164], intramolecular planarization [165], twisting intramolecular charge transfer [166], and hydrogen-bonding [167]. We tackle the AIE issue by quantitatively computing the radiative and non-radiative decay rates for molecule and in aggregate, to look at the light emitting quantum efficiency: $\eta = \frac{k_r}{k_r+k_{nr}}$. Namely, our interest is how aggregate influences η. The molecules investigated are listed in Fig. 15.

Table 5 summarizes the calculated radiative decay and internal conversion rates and the corresponding fluorescence quantum efficiencies for a series of conventional novel AIE-active and AIE-active fluorophors (specified in the Table). These have been obtained in our previous work [54,168–172]. It should be noted that the ISC rates were not included in computing these molecular fluorescence quantum efficiency because of the extremely small spin–orbit coupling as well as a number of experimental observations that: (i) for three diphenylbutadiene (DPB), the quantum yields of intersystem crossing are all lower than 0.02; [173,174] (ii) the phosphorescence emission is very weak [175], even not detectable in perylene and there is no observable transition from S_1 to triplet state in terrylene [176]; (iii) the other AIE-active compounds all exhibit strongly fluorescence at low temperature and do not show any phosphorescence [177–179], which all rationalize the neglect of the ISC rates for these compounds.

From Table 5, we can conclude that (i) not only the calculated rates but also the quantum efficiencies are in nice agreements with the available experimental results, which further verify both our vibration correlation function method and DFT/TDDFT calculation for the lowest excited state are reliable, allowing quantitatively to predict the luminescent properties of organic molecules; (ii) the radiative decay rates vary 2 orders of magnitude ranging from $\sim 10^6$ to $\sim 10^8$ s^{-1} for different compounds; while the IC rates vary vastly from $\sim 10^3$ to $\sim 10^{12}$ s^{-1}; (iii) the single AIE-active molecules hardly exhibit fluorescence at room temperature, due to the usually large internal conversion rates than the radiative decay rates. This is closed correlated with the fact that the HR-factors are much larger than those of the fluorescence molecules, say perylene and terrylene.

Internal conversion rate is very sensitive to the energy gap and the reorganization energy. Reorganization energy λ_k from the kth normal mode is defined as the product of its energy $\hbar\omega_k$ and the corresponding Huang–Rhys factor HR_k, $\lambda_k = \hbar\omega_k \mathrm{HR}_k = \omega_k^2 \Delta Q_k^2/2$ which is a direct measurement for the extent of vibronic coupling between two electronic states. We apply the short time approximation for strong coupling $\sum_k S_k \gg 1$,

$$e^{\pm i\omega_k t} = 1 \pm i\omega_k t - \frac{\omega_k^2 t^2}{2} + \cdots. \tag{96}$$

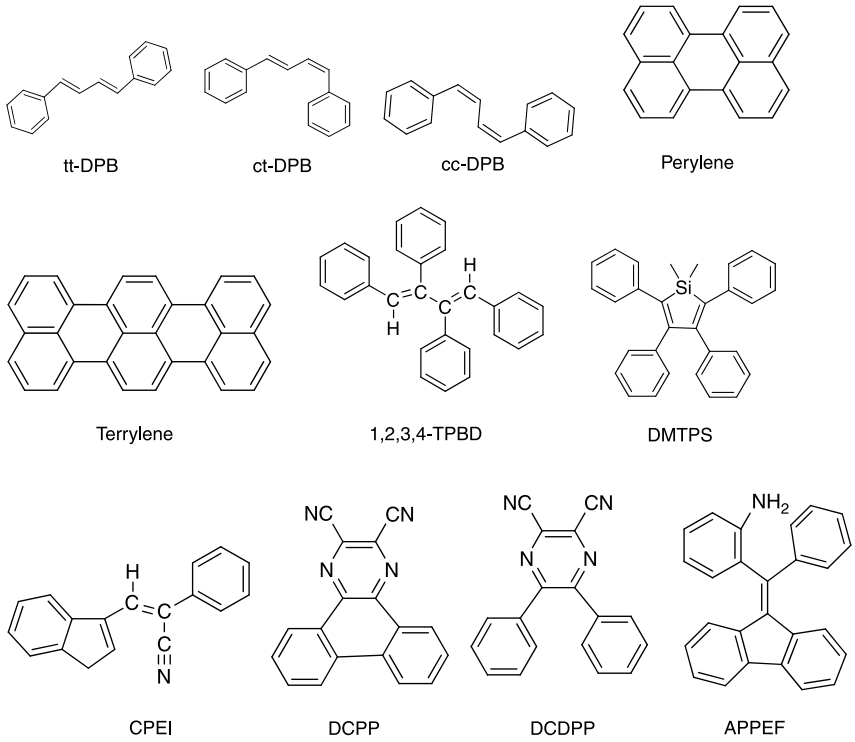

Fig. 15. Molecular structures of the traditional and novel AIE-active fluorophors.

Assuming there is only one promoting mode contributing to the electronic coupling term, and ignoring the mode-mixing effect, we may write down the rate as:

$$k_{\mathrm{IC},I} = \frac{1}{\hbar^2}\left(\frac{\omega_I}{2\hbar}\,|R_I|^2\right)\sqrt{\frac{\pi}{\sum_k{}' \lambda_k \bar{E}_k}}\exp\left[-\frac{\left(E_{\mathrm{if}} - \hbar\omega_I - \sum_k{}' \lambda_k\right)^2}{4\sum_k{}' \lambda_k \bar{E}_k}\right]. \tag{97}$$

The following quadratic equation can be deduced

$$\ln k_{\mathrm{IC},I} = -\frac{\left[E_{\mathrm{if}} - \left(\hbar\omega_I + \sum_k{}' \lambda_k\right)\right]^2}{4\sum_k{}' \lambda_k \bar{E}_k} + \ln\left(\frac{1}{\hbar^2}\left(\frac{\omega_I}{2\hbar}\,|R_I|^2\right)\sqrt{\frac{\pi}{\sum_k{}' \lambda_k \bar{E}_k}}\right), \tag{98}$$

where $\bar{E}_k = (\bar{n}_k + 1/2)\hbar\omega_k$ is the average vibration energy of the kth mode, and $\bar{n}_k = (\exp(\hbar\omega_k/kT) - 1)^{-1}$ is the average phonon number. The right hand side is a downside parabola with a maximum at $E_{\mathrm{if}} = \sum_k{}' \lambda_k + \hbar\omega_I$. It is also seen that with increasing reorganization energy, the parabola gets wider and wider.

We may plot the rate as a function of energy gap for the ACQ-active DCPP and AIE-active DCDPP at 300 K as an example, in Fig. 16. It is seen that the curve for DCDPP is much wider than DCPP: the former possesses much larger reorganization energy. Thus, even though their transition energies are close each other, the rate of DCDPP is about four orders of magnitude larger than that of DCPP, which strongly deviate from the energy gap law.

It is quite impressive that the data reported in Table 5 are in general in agreement with the measurements, even though the model adopted here was based on displaced and distorted harmonic oscillators. One can imagine that for the non-adiabatic transition between the excited state and the ground state, the conversion of electronic energy into vibration degrees of freedom should involve a large number of vibration quanta, leading to remarkable anharmonicity. Indeed, for a diatomic molecule with only one degree of freedom (the bond stretching as the vibration mode), the dissipation of electronic excited state energy into vibration leads to enormous anharmonic effect. For a polyatomic conjugated molecule, first the electronic excitation energy is decreased due to the size effect, secondly, the number of normal modes increases, to share the decreased electronic energy. The average quanta involved by one mode become much less than that of the

Table 5
Summary of the largest Huang–Rhys factors (HR_Max), the electric transition dipole moments, the radiative decay rate, the non-radiative decay rate and the corresponding fluorescence quantum efficiency, as well as the available experimental data in parenthesis.

	HR_ Max	μ/Debye	k_r /s^{-1}	k_{IC}/s^{-1}	Φ_F
tt-DPB	0.43	11.57	9.58×10^8 ($1.4\sim9.0 \times 10^8$)[a] ($5\sim7 \times 10^8$)[b]	1.19×10^9 ($0.6\sim6.2 \times 10^9$)[a] ($0.8\sim1.8 \times 10^9$)[c]	0.44 (0.42)[b]
ct-DPB	3.60	9.54	6.64×10^8	2.84×10^{12}	2.34×10^{-4} ($<10^{-3}$)[d]
cc-DPB	5.08	9.98	7.74×10^8	9.16×10^{11}	8.44×10^{-4} ($<10^{-3}$)[d]
Perylene	0.35	6.09	0.91×10^8	0.72×10^3	1.0 ($\sim$1.0)[e]
Terrylene	0.35	9.89	1.20×10^8	0.51×10^5	1.0 ($\sim$1.0)[e]
DCPP	0.88	1.03	1.59×10^6	3.29×10^5	0.83 ($\sim$)
DCDPP (AIE-active)	5.80	2.87	0.93×10^7	4.45×10^9	2.09×10^{-3} (1.5×10^{-4})[f]
CPEI (AIE-active)	6.26	7.45	0.61×10^8	3.28×10^{11}	1.86×10^{-4} (<0.001)[g]
1, 2, 3, 4-TPBD (AIE-active)	47.74	8.27	4.80×10^8	1.09×10^{10}	0.042 (1.1×10^{-3})[h]
DMTPS (AIE-active)	31.84	5.60	1.20×10^8	1.80×10^{11}	6.66×10^{-4} (2.2×10^{-4})[i]
APPEF (AIE-active)	34.35	3.23	0.47×10^6	1.27×10^8	3.69×10^{-3} (1.1×10^{-3})[j]

[a] Ref. [180], measured in different solvents.
[b] Ref. [181] in 3-methylpentane.
[c] Ref. [180] in 3-methylpentane.
[d] Ref. [174].
[e] Ref. [182–184].
[f] Ref. [178] in tetrahydrofuran.
[g] Ref. [177].
[h] Ref. [185] in acetone.
[i] Ref. [186] in cyclohexane.
[j] Ref. [179] in acetonitrile.

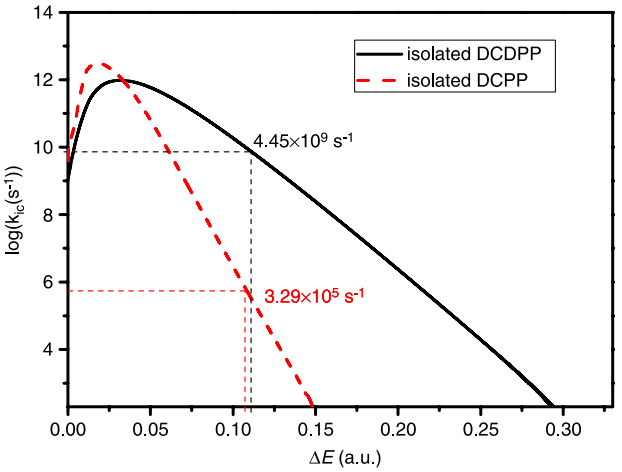

Fig. 16. The internal conversion rate versus the energy gap for DCDPP and DCPP: a similar gap but huge different rate, highlighting the role of reorganization energy.

diatomic molecule. It has been shown when elongating the oligomer length, the vibrational quanta of the promoting mode corresponding to the maximum internal conversion rate decreases steadily [150], rationalizing the applicability of harmonic model.

Now, we look at the aggregation effect by employing the QM/MM approach. Here AIE-active DCDPP is chosen as an example to investigate the effect of molecular aggregation on the photophysical properties [54]. We cut a cluster of 18 molecules from the X-ray diffraction crystal structure [178] to set up our computational model (Fig. 17), which consists of 32 QM atoms and 544 MM atoms. Coupled with the DFT and TDDFT, using the vibrational correlation function method the

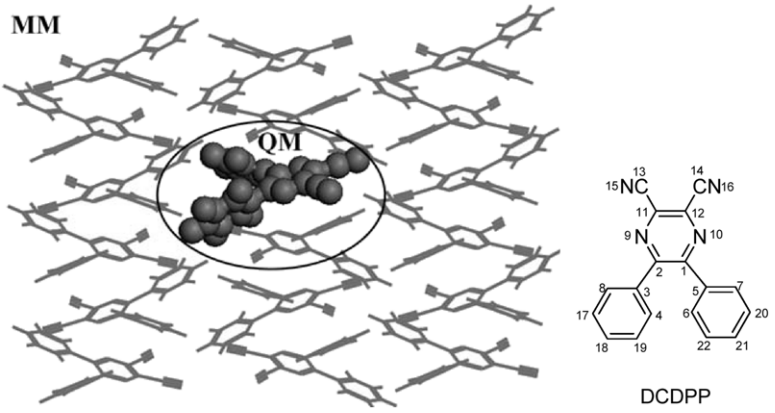

Fig. 17. QM/MM computational model for DCDPP cluster with 18 molecules and the atom-labeling scheme is shown at the right.
Source: Reprinted figure with permission from Ref. [54].

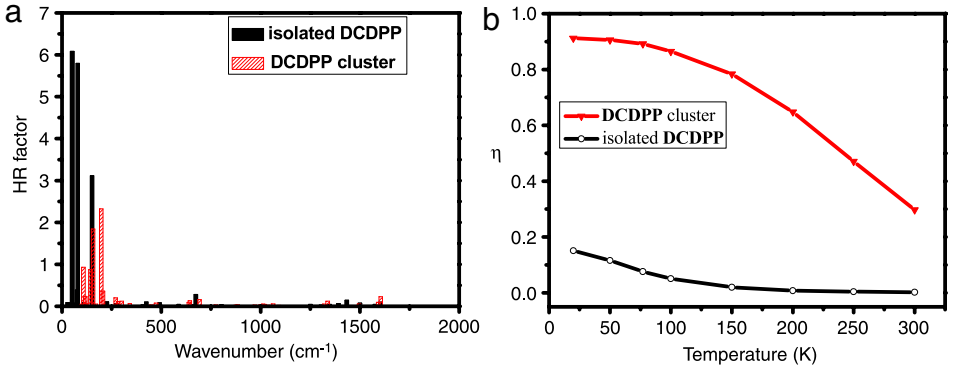

Fig. 18. (a) Huang–Rhys factors and (b) fluorescence quantum efficiency in the whole range of temperature, for both isolated (black line) and aggregate (red line) **DCDPP** molecules. (For interpretation of the references to colour in this figure legend, the reader is referred to the web version of this article.)

radiative and non-radiative decay rates were calculated to be 7.55×10^6 s^{-1} and 1.78×10^7 s^{-1} at 300 K, respectively. Compared with the rates of isolated DCDPP given in Table 5, the radiative rate hardly varies, from 9.32×10^6 s^{-1} to 7.55×10^6 s^{-1}; while the non-radiative decay rate sharply decreases two orders of magnitude, from 4.45×10^9 to 1.78×10^7 s^{-1}, which is strongly influenced by molecular aggregation. Consequently, in the gas phase or dilute solution, the fluorescence quantum efficiency is as low as 0.002. While in aggregation state, the radiative can compete with the non-radiative rate and the molecule exhibits strongly fluorescent with quantum efficiency of 0.30, in agreement with experiment.

From Fig. 18(a), we can see that upon aggregation, the couplings of low frequency modes with electron excitation are suppressed. This is precisely the reason causing the aggregation effect on the fluorescence quantum efficiency, namely, the dissipation channels through the phenyl twisting are suppressed, allowing more chances for the radiative decay in **DCDPP**. For more details, we list the decay rates for both **DCPP** (Table 6) and **DCDPP** (Table 7) for a comparing isolated molecule and molecule-in-cluster at different temperature. It is seen that the aggregation effect on **DCPP** is minor.

5. Conclusion and perspectives

Electroluminescent molecules and polymers continue to attract intensive attentions. We have emphasized three aspects relating to the light-emitting phenomena in theoretical and computational study for OLEDs materials. First, the nature of the lowest excited state, its symmetry and oscillator strength, dictates emissiveness. The electronic excited state remains a major challenge in computational chemistry, especially when the multi-reference contribution is important, such as the $2A_g$ state. Multi-reference configuration interaction (MRCI) plus perturbation correction is so far the most reliable approach. Unfortunately, it is quite a costly method, limiting to molecules with about 10 heavy atoms. Equation of motion at the coupled-cluster level (EOM/CC) is another choice, though higher than double excitations are often required to guarantee the accuracy, which suffers the same limitation for small molecule. Recent advances in DMRG have much improved both the accuracy and efficiency [71]. Our proposed DMRG was based on semiempirical quantum chemistry model, which strongly

Table 6
The calculated radiative decay rate (k_r) and non-radiative decay rate (k_{nr}) and the fluorescence quantum yield (η_f) for the **DCPP**.

T [K]	Molecule-in-cluster			Isolated molecule		
	k_r (s^{-1})	k_{nr} (s^{-1})	η_f	k_r (s^{-1})	k_{nr} (s^{-1})	η_f
300	1.64×10^6	8.37×10^5	0.66	1.59×10^6	3.29×10^5	0.83
250	1.71×10^6	5.12×10^5	0.77	1.60×10^6	2.74×10^5	0.85
200	1.78×10^6	3.30×10^5	0.84	1.61×10^6	2.42×10^5	0.87
150	1.85×10^6	2.26×10^5	0.89	1.61×10^6	2.25×10^5	0.88
100	1.90×10^6	1.68×10^5	0.92	1.62×10^6	2.15×10^5	0.88
77	1.93×10^6	1.52×10^5	0.93	1.62×10^6	2.13×10^5	0.88
50	1.94×10^6	1.40×10^5	0.93	1.62×10^6	2.11×10^5	0.88
20	1.95×10^6	1.36×10^5	0.93	1.62×10^6	2.09×10^5	0.89

Table 7
The calculated radiative decay rate (k_r) and non-radiative decay rate (k_{nr}) and the fluorescence quantum yield (η_f) for the **DCDPP**.

T [K]	Cluster			Isolated molecule		
	k_r (s^{-1})	k_{nr} (s^{-1})	η_f	k_r (s^{-1})	k_{nr} (s^{-1})	η_f
300	7.55×10^6	1.78×10^7	0.30	9.32×10^6	4.45×10^9	0.21×10^{-2}
250	7.95×10^6	8.96×10^6	0.47	9.83×10^6	2.44×10^9	0.40×10^{-2}
200	8.34×10^6	4.50×10^6	0.65	1.04×10^7	1.21×10^9	0.85×10^{-2}
150	8.70×10^6	2.36×10^6	0.78	1.09×10^7	5.32×10^8	0.02
100	9.03×10^6	1.37×10^6	0.87	1.14×10^7	2.14×10^8	0.05
77	9.15×10^6	1.12×10^6	0.89	1.16×10^7	1.40×10^8	0.08
50	9.26×10^6	9.58×10^5	0.91	1.18×10^7	9.01×10^7	0.12
20	9.30×10^6	9.04×10^5	0.91	1.20×10^7	6.75×10^7	0.15

relied on parameterization. TDDFT is working well when the lowest excited state is indeed an ionic excitation. In that case, the challenge lies in the electron dynamics coupled with nuclear motion. The dynamics simulation for electron requires a time step in the order of attosecond, while for nuclear at the femtosecond. The total simulation time is limited to tens of picoseconds, far short for understanding light-emitting property, since the radiative decay time is typically longer than nanosecond, or even longer for phosphorescence. Especially, the quantum nature of the nuclear motion often plays crucial role in electron dynamics. The proposed rate formalism in this work captures the essential quantum feature of nuclear vibration, but is limited to harmonic model, both anharmonic effects and dynamics are lacking. Nevertheless, such an approach indeed gave satisfactory results for both the optical spectra and the radiative and non-radiative decay rates, justifying the applicability for modeling OLEDs materials. As for the electroluminescent process, there has been a long-standing controversy over whether there existed spin statistical limit of 25% for the singlet exciton formation portion. From both the electronic coupling and the driving force consideration during the charge recombination process, we conclude that such limit can be beaten up! In addition to the supports from photophysics data, recent advances in blue OLEDs materials and devices demonstrated undoubtedly that the singlet portion can go up to 62.5% for pure electro-fluorescence [117].

We have identified three theoretical issues in OLEDs, the symmetry of the lowest excited state, the spin-dependent exciton formation, and the competition of radiative and non-radiative decays. We make the following summarizations to conclude this Report: (i) The symmetrized DMRG works well for the optical related properties, including targeting the excited state with high precision and we have demonstrated a quantum confinement effect on the excited state 1B/2A ordering and crossover; (ii) A direct extension of DMRG to long-range interaction taking polyenes as example, indicated that the accuracy is still kept if the interaction is diagonal such as the density–density terms, allowing application to semiempirical quantum chemistry; (iii) Exciton formation is viewed as an interchain charge recombination process, and it is found that the polaron pair possesses negligible exchange energy, allowing singlet and triplet loosely bound pair to interchange each other; (iv) The charge recombination to form singlet exciton is in general faster than the triplet because the driving force (gap) is larger for triplet as well as the electronic coupling is larger for singlet due to the interchain bond-charge correlation effect; (v) A general rate formalism based on vibration correlation function is developed here combining both non-adiabatic and spin–orbit couplings, which gave satisfactory results in comparison with experiments for light-emitting molecules and polymers. Both the computational efficiency and accuracy for calculating the absorption and emission spectra have been shown to be excellent; (vi) The exotic aggregation induced mission phenomena is explained based on non-radiative decay blocking picture, namely, the molecular aggregate tends to hinder the vibration dissipation of the electronic excitation energy, while leaving the radiative decay process relatively untouched.

Excited state structure and processes will be continuing to be challenging for both computational chemistry and physics, not only for the reason of pressing application in optoelectronic devices or energy materials, but also for the fundamental difficulty [187]. Both electron–electron correlation and electron–phonon couplings are required for even a

basic understanding. These many-body effects have been central issues for condensed matter physics since decades and now with the great advances of computational techniques, numerical approximate solutions become more and more feasible for electron correlation [188] and electron–phonon couplings [189].

Acknowledgments

The authors are acknowledging here the essential contributions from the following collaborators: Profs. David Beljonne, Jean-Luc Brédas, Swapan Pati, Surja Ramasesha, Jiushu Shao, as well as the following group members: Drs. Shiwei Yin, Yingli Niu, Liping Chen, Qunyan Wu, and Ms. Yuqian Jiang. The work is supported by the National Science Foundation of China (Grant Nos. 21290191, 91233105, and 91333202) and the "973" program of the Ministry of Science and Technology of China (Grant Nos. 2013CB834703, 2011CB932304, 2011CB808405, and 2013CB933503).

References

[1] C.W. Tang, S.A. Van Slyke, Appl. Phys. Lett. 51 (1987) 913.
[2] J.H. Burroughes, D.D.C. Bradley, A.R. Burn, R.N. Marks, K. Mackay, R.H. Friend, A.B. Holmes, Nature 347 (1990) 539.
[3] G. Horowitz, Adv. Mater. 10 (1998) 365.
[4] G. Yu, J. Gao, J.C. Hummelen, F. Wudl, A.J. Heeger, Science 270 (1995) 1789.
[5] B.S. Gaylord, A.J. Heeger, G.C. Bazan, Proc. Natl. Acad. Sci. USA 99 (2002) 10954.
[6] Z.H. Xiong, D. Wu, Z.V. Vardeny, J. Shi, Nature 427 (2004) 821.
[7] V.A. Dediu, L.E. Hueso, I. Bergenti, C. Taliani, Nature Mater. 8 (2009) 707.
[8] A. Kohler, D.A. dos Santos, D. Beljonne, Z. Shuai, J.L. Bredas, A.B. Holmes, A. Kraus, K. Muellen, R.H. Friend, Nature 392 (1998) 903.
[9] M. Kasha, Discuss Faraday Soc. 9 (1950) 14.
[10] B.S. Hudson, B.E. Kohler, Chem. Phys. Lett. 14 (1972) 299.
[11] I. Ohmine, M. Karplus, K. Schulten, J. Chem. Phys. 68 (1978) 2298.
[12] Z.G. Soos, D.S. Galvao, S. Etemad, Adv. Mater. 6 (1994) 280.
[13] P. Tavan, K. Schulten, Phys. Rev. B 36 (1987) 4337.
[14] S. Ramasesha, Z.G. Soos, J. Chem. Phys. 80 (1984) 3278.
[15] Z.G. Soos, Y.A. Pati, S.K. Pati, J. Chem. Phys. 112 (2000) 3133.
[16] Z.G. Shuai, J.L. Brédas, Phys. Rev. B 62 (2000) 15452.
[17] R.G. Parr, W. Yang, Density-Functional Theory of Atoms and Molecules, Oxford University Press, New York, 1989.
[18] N.T. Maitra, F. Zhang, R.J. Cave, K. Burke, J. Chem. Phys. 120 (2004) 5932.
[19] J. Hubbard, Proc. R. Soc. A-Math. Phys. Eng. Sci. 276 (1963) 238.
[20] (a) R. Pariser, R.G. Parr, J. Chem. Phys. 21 (1953) 466;
(b) J.A. Pople, Trans. Faraday Soc. 49 (1953) 1375.
[21] S.R. White, Phys. Rev. Lett. 69 (1992) 2863.
[22] S. Ramasesha, S.K. Pati, H.R. Krishnamurthy, Z.G. Shuai, J.L. Brédas, Phys. Rev. B 54 (1996) 7598.
[23] Z.G. Shuai, J.L. Brédas, S.K. Pati, S. Ramasesha, Proc. SPIE—Int. Soc. Opt. Eng. 3145 (1997) 293.
[24] Z.G. Shuai, J.L. Brédas, A. Saxena, A.R. Bishop, J. Chem. Phys. 109 (1998) 2549.
[25] R.H. Friend, R.W. Gymer, A.B. Holmes, J.H. Burroughes, R.N. Marks, C. Taliani, D.D.C. Bradley, D.A. Dos Santos, J.L. Brédas, M. Logdlund, W.R. Salaneck, Nature 397 (1999) 121.
[26] Y.G. Ma, H.Y. Zhang, J.C. Shen, C.M. Che, Synth. Met. 94 (1998) 245.
[27] M.A. Baldo, D.F. O'Brien, Y. You, A. Shoustikov, S. Sibley, M.E. Thompson, S.R. Forrest, Nature 395 (1998) 151.
[28] C. Adachi, M.A. Baldo, M.E. Thompson, S.R. Forrest, J. Appl. Phys. 90 (2001) 5048.
[29] Y. Cao, I.D. Parker, G. Yu, C. Zhang, A.J. Heeger, Nature 397 (1999) 414.
[30] Z.G. Shuai, D. Beljonne, R.J. Silbey, J.L. Brédas, Phys. Rev. Lett. 84 (2000) 131.
[31] T.D. Nguyen, G. Hukic-Markosian, F.J. Wang, L. Wojcik, X.G. Li, E. Ehrenfreund, Z.V. Vardeny, Nature Mater. 9 (2010) 345.
[32] B. Hu, Y. Wu, Nature Mater. 6 (2007) 985.
[33] D.L. Sun, L.F. Yin, C.J. Sun, H.W. Guo, Z. Gai, X.G. Zhang, T.Z. Ward, Z.H. Cheng, J. Shen, Phys. Rev. Lett. 104 (2010) 236602.
[34] M. Lax, J. Chem. Phys. 20 (1952) 1752.
[35] R. Kubo, Phys. Rev. 86 (1952) 929.
[36] Y.J. Yan, S. Mukamel, J. Chem. Phys. 85 (1986) 5908.
[37] R. Ianconescu, E. Pollak, J. Phys. Chem. 108 (2004) 7778.
[38] Y. He, E. Pollak, J. Phys. Chem. A 105 (2001) 10961.
[39] Y.L. Niu, Q. Peng, C.M. Deng, X. Gao, Z.G. Shuai, J. Phys. Chem. 114 (2010) 7817.
[40] R. Borrelli, A. Capobianco, A. Peluso, J. Phys. Chem. A 116 (2012) 9934.
[41] M.H. Beck, A. Jäckle, G.A. Worth, H.D. Meyer, Phys. Rep. 324 (2000) 1.
[42] Z. Lan, E. Fabiano, W. Thiel, J. Phys. Chem. B 113 (2009) 3548.
[43] P.A. Hunt, M.A. Robb, J. Am. Chem. Soc. 127 (2005) 5720.
[44] T. Nelson, S. Fernandez-Alberti, V. Chernyak, A.E. Roitberg, S. Tretiak, J. Phys. Chem. B 115 (2011) 5402.
[45] C.F. Craig, W.R. Duncan, O.V. Prezhdo, Phys. Rev. Lett. 95 (2005) 163001.
[46] G.A. Worth, H.D. Meyer, H. Köppel, L.S. Cederbaum, I. Burghardt, Int. Rev. Phys. Chem. 27 (2008) 569.
[47] S. Hammes-Schiffer, Chem. Rev. 110 (2010) 6937.
[48] X. Sun, W.H. Miller, J. Chem. Phys. 106 (1997) 6346.
[49] K. Huang, A. Rhys, Proc. Roy. Soc. Lond. A 204 (1950) 406.
[50] S.H. Lin, J. Chem. Phys. 44 (1966) 3759.
[51] R. Englmann, J. Jortner, Mol. Phys. 18 (1970) 145.
[52] Q. Peng, Y.P. Yi, Z.G. Shuai, J.S. Shao, J. Chem. Phys. 126 (2007) 114302.
[53] Q. Peng, Y.L. Niu, Q.H. Shi, X. Gao, Z.G. Shuai, J. Chem. Theory. Comput. 9 (2013) 1132.
[54] Q.Y. Wu, C.M. Deng, Q. Peng, Y.L. Niu, Z.G. Shuai, J. Comput. Chem. 33 (2012) 1862.
[55] E.H. Lieb, F.Y. Wu, Phys. Rev. Lett. 20 (1968) 1445.
[56] C.N. Yang, C.P. Yang, J. Math. Phys. 10 (1969) 1115.
[57] A.A. Ovchinikov, Sov. Phys.—JETP 30 (1970) 1160.
[58] F.C. Zhang, T.M. Rice, Phys. Rev. B 37 (1988) 3759.
[59] F.D.M. Haldane, Phys. Rev. Lett. 50 (1983) 1153.
[60] S. Ramasesha, Z.G. Soos, J. Chem. Phys. 80 (1984) 3278.

[61] Z.G. Soos, S. Ramasesha, Phys. Rev. B 29 (1984) 5410.
[62] S.N. Dixit, D. Guo, S. Mazumdar, Phys. Rev. B 43 (1991) 6781.
[63] Z.G. Shuai, S.K. Pati, W.P. Su, J.L. Brédas, S. Ramasesha, Phys. Rev. B 55 (1997) 15368.
[64] D. Yaron, E.E. Moore, Z.G. Shuai, J.L. Brédas, J. Chem. Phys. 108 (1998) 7451.
[65] K. Ohno, Theor. Chim. Acta 2 (1964) 219.
[66] G. Klopman, J. Am. Chem. Soc. 86 (1964) 4550.
[67] S.R. White, D.J. Scalapino, Phys. Rev. Lett. 80 (1998) 1272.
[68] G. Fano, F. Ortolani, L. Ziosi, J. Chem. Phys. 108 (1998) 9246.
[69] S.R. White, R.L. Martin, J. Chem. Phys. 110 (1999) 4127.
[70] K.H. Marti, M. Reiher, Mol. Phys. 108 (2010) 501.
[71] G.K.L. Chan, S. Sharma, Ann. Rev. Phys. Chem. 62 (2011) 465.
[72] Z.G. Shuai, J.L. Brédas, S.K. Pati, S. Ramasesha, Phys. Rev. B 56 (1997) 9298.
[73] Z.G. Soos, S. Ramasesha, D.S. Galvão, Phys. Rev. Lett. 71 (1993) 1609.
[74] R.E. Martin, U. Gubler, J. Cornil, M. Balakina, C. Boudon, C. Bosshard, J.P. Gisselbrecht, F. Diederich, P. Guenter, M. Gross, J.L. Bredas, Chem. Eur. J. 6 (2000) 3622.
[75] I. Gontia, S.V. Frolov, M. Liess, E. Ehrenfreund, Z.V. Vardeny, K. Tada, H. Kajii, R. Hidayat, A. Fujii, K. Yoshino, M. Teraguchi, T. Masuda, Phys. Rev. Lett. 82 (1999) 4058.
[76] A. Sugita, T. Kobayashi, Chem. Phys. Lett. 346 (2001) 41.
[77] D. Bloor, and R. R. Chance (Eds.), Polydiacetylene, NATO ASIE 102, (Nijhoff, The Hague, 1985).
[78] R.J.O.M. Hoofman, L.D.A. Siebbeles, M.P. de Haas, A. Hummel, D. Bloor, J. Chem. Phys. 109 (1998) 1885.
[79] L.P. Chen, X.J. Hou, L.Y. Zhu, S.W. Yin, Z.G. Shuai, J. Theot. Comput. Chem. 5 (2006) 391.
[80] N.S. Sariciftci (Ed.), Primary Photoexcitations in Conjugated Polymers: Molecular Exciton versus Semiconductor Band Model, World Scientific, Singapore, 1997.
[81] N. Chawdhury, A. Köhler, R.H. Friend, W.-Y. Wong, J. Lewis, M. Younus, P.R. Raithby, T.C. Corcoran, M.R.A. Al-Mandhary, M.S. Khan, J. Chem. Phys. 110 (1999) 4963.
[82] A. Köhler, J.S. Wilson, R.H. Friend, M.K. Al-Suti, M.S. Khan, A. Gerhard, H. Bässler, J. Chem. Phys. 116 (2002) 9457.
[83] A.P. Monkman, H.D. Burrows, L.J. Hartwell, L.E. Horsburgh, I. Hamblett, S. Navaratnam, Phys. Rev. Lett. 86 (2001) 1358.
[84] Y.V. Romanovskii, A. Gerhard, B. Schweitzer, U. Scherf, R.I. Personov, H. Bässler, Phys. Rev. Lett. 84 (2000) 1027.
[85] D. Hertel, S. Setayesh, H.G. Nothofer, U. Scherf, K. Muellen, H. Bässler, Adv. Mater. 13 (2001) 65.
[86] D. Beljonne, Z. Shuai, R.H. Friend, J.L. Brédas, J. Chem. Phys. 102 (1995) 2042.
[87] M. Segal, M.A. Baldo, R.J. Holmes, S.R. Forrest, Z.G. Soos, Phys. Rev. B 68 (2003) 075211.
[88] P.K.H. Ho, J. Kim, J.H. Burroughes, H. Becker, S.F.Y. Li, T.M. Brown, F. Cacialli, R.H. Friend, Nature 404 (2000) 481.
[89] J.S. Wilson, A.S. Dhoot, A.J.A.B. Seeley, M.S. Khan, A. Köhler, R.H. Friend, Nature 413 (2001) 828.
[90] M. Wohlgenannt, X.M. Jiang, Z.V. Vardeny, R.A.J. Janssen, Phys. Rev. Lett. 88 (2002) 197401.
[91] A.S. Dhoot, D.S. Ginger, D. Beljonne, Z. Shuai, N.C. Greenham, Chem. Phys. Lett. 360 (2002) 195.
[92] T. Virgili, G. Cerullo, L. Lüer, G. Lanzani, C. Gadermaier, D.D.C. Bradley, Phys. Rev. Lett. 90 (2003) 247402.
[93] E.A. Meulenkamp, R. van Aar, J.J.A.M. Bastiaansen, A.J.M. van den Biggelaar, H. Börner, K. Brunner, M. Büchel, A. van Dijken, N.M.M. Kiggen, M. Kilitziraki, M.M. de Kok, B.M.W. Langeveld, M.P.H. Ligter, S.I.E. Vulto, P. van de Weijer, S.H.P.M. de Winter, SPIE—Int. Soc. Opt. Eng. 5464 (2004) 90–103.
[94] A. Ye, Z.G. Shuai, J.L. Brédas, Phys. Rev. B 65 (2002) 045208.
[95] M.N. Kobrak, E.R. Bittner, Phys. Rev. B 62 (2000) 11473.
[96] S. Karabunarliev, E.R. Bittner, Phys. Rev. Lett. 90 (2003) 057402.
[97] K. Tandon, S. Ramasesha, S. Mazumdar, Phys. Rev. B 67 (2003) 045109.
[98] T. Hong, H. Meng, Phys. Rev. B 63 (2003) 075206.
[99] M.A. Baldo, D.F. O'Brien, M.E. Thompson, S.R. Forrest, Phys. Rev. B 60 (1999) 14422.
[100] E.L. Frankevich, A.A. Lymarev, I. Sokolik, F.E. Karasz, S. Blumstengel, R.H. Baughman, H.H. Hörhold, Phys. Rev. B 46 (1992) 9320.
[101] V. Dyakonov, G. Rösler, M. Schwoerer, E.L. Frankevich, Phys. Rev. B 56 (1997) 3852.
[102] A. Kadashchuk, A. Vakhnin, I. Blonski, D. Beljonne, Z. Shuai, J.L. Brédas, V.I. Arkhipov, P. Heremans, E.V. Emelianova, H. Bässler, Phys. Rev. Lett. 93 (2004) 066803.
[103] S. Kivelson, W.P. Su, J.R. Schrieffer, A.J. Heeger, Phys. Rev. Lett. 58 (1987) 1899.
[104] M.J. Rice, Yu.N. Gartstein, Phys. Rev. B 53 (1996) 10764.
[105] D. Beljonne, A. Ye, Z. Shuai, J.L. Brédas, Adv. Funct. Mater. 14 (2004) 684.
[106] R.A. Marcus, J. Chem. Phys. 43 (1965) 679.
[107] K. Tandon, S. Ramasesha, S. Mazumdar, Phys. Rev. B 67 (2003) 045109.
[108] S. Karabunarliev, E.R. Bittner, Phys. Rev. Lett. 90 (2003) 057402.
[109] L.P. Chen, L.Y. Zhu, Z.G. Shuai, J. Phys. Chem., A 110 (2006) 13349.
[110] M. Wohlgenannt, K. Tandon, S. Mazumdar, S. Ramasesha, Z.V. Vardeny, Nature 409 (2001) 494.
[111] M.K. Lee, M. Segal, Z.G. Soos, J. Shinar, M.A. Baldo, Phys. Rev. Lett. 94 (2005) 137403.
[112] M. Reufer, M.J. Walter, P.G. Lagoudakis, A.B. Hummel, J.S. Kolb, H.G. Roskos, U. Scherf, J.M. Lupton, Nature Mater. 4 (2005) 340.
[113] D. Moses, J. Wang, A.J. Heeger, N. Kirova, S. Brazovski, Synth. Met. 125 (2002) 93.
[114] S.V. Frolov, Z. Bao, M. Wohlgenannt, Z.V. Vardeny, Phys. Rev. Lett. 85 (2000) 2196.
[115] R.N. Marks, J.J.M. Halls, D.D.C. Bradley, R.H. Friend, A.B. Holmes, J. Phys.: Condens. Matter 6 (1994) 1379.
[116] M. Deussen, M. Scheidler, H. Bässler, Synth. Met. 73 (1995) 123.
[117] C.G. Zhen, Z.K. Chen, Q.D. Liu, Y.F. Dai, R.Y.C. Shin, S.Y. Chang, J. Kieffer, Adv. Mater. 21 (2009) 2425.
[118] C.G. Zhen, Y.F. Dai, W.J. Zeng, Z. Ma, Z.K. Chen, J. Kieffer, Adv. Funct. Mater. 21 (2011) 699.
[119] H. Uoyama, K. Goushi, K. Shizu, H. Nomura, C. Adachi, Nature 492 (2012) 234.
[120] F.C. Spano, Acc. Chem. Res. 43 (2010) 429.
[121] L.D. Bakalis, J. Knoester, J. Phys. Chem. B 103 (1999) 6620.
[122] J. Gierschner, L. Lüer, D. Oelkrug, E. Musluoglu, B. Behnisch, M. Hanack, Adv. Mater. 12 (2000) 757.
[123] A.Y. Dymarsky, K.N. Kudin, J. Chem. Phys. 122 (2005) 124103.
[124] F. Duschinsky, Acta Physicochimica URSS 7 (1937) 551.
[125] S.H. Lin, C.H. Chang, K.K. Liang, R. Chang, Y.J. Shiu, J.M. Zhang, M. Hayashi, F.C. Hsu, Advances in Chemical Physics, vol. 122, John Wiley & Sons, New York, 2002, pp. 1–88.
[126] Y.L. Niu, Q. Peng, Z.G. Shuai, Sci. China B: Chem. 51 (2008) 1153.
[127] H.J. Werner, P.J. Knowles, R. Lindh, F.R Manby, M. Schutz, A. Others, MOLPRO, Version 2009.1, A Package of ab Initio Programs, University College Cardiff Consultants Limited, Cardiff, 2009, available online: http://www.molpro.net.
[128] P. Deglmann, F. Furche, R. Ahlrichs, Chem. Phys. Lett. 362 (2002) 511.

[129] M.J. Frisch, G.W. Trucks, H.B. Schlegel, G.E. Scuseria, M.A. Robb, J.R. Cheeseman, G. Scalmani, V. Barone, B. Mennucci, G.A. Petersson, H. Nakatsuji, M. Caricato, X. Li, H.P. Hratchian, A.F. Izmaylov, J. Bloino, G. Zheng, J.L. Sonnenberg, M. Hada, M. Ehara, K. Toyota, R. Fukuda, J. Hasegawa, M. Ishida, T. Nakajima, Y. Honda, O. Kitao, H. Nakai, T. Vreven, J.A. Montgomery, J.E. Peralta, F. Ogliaro, M. Bearpark, J.J. Heyd, E. Brothers, K.N. Kudin, V.N. Staroverov, R. Kobayashi, J. Normand, K. Raghavachari, A. Rendell, J.C. Burant, S.S. Iyengar, J. Tomasi, M. Cossi, N. Rega, J.M. Millam, M. Klene, J.E. Knox, J.B. Cross, V. Bakken, C. Adamo, J. Jaramillo, R. Gomperts, R.E. Stratmann, O. Yazyev, A.J. Austin, R. Cammi, C. Pomelli, J.W. Ochterski, R.L. Martin, K. Morokuma, V.G. Zakrzewski, G.A. Voth, P. Salvador, J.J. Dannenberg, S. Dapprich, A.D. Daniels, Ö. Farkas, J.B. Foresman, J.V. Ortiz, J. Cioslowski, D.J. Fox, Gaussian Inc.: Wallingford C T (2009).
[130] Y.H. Shao, L.F. Molnar, Y. Jung, J. Kussmann, C. Ochsenfeld, S.T. Brown, A.T.B. Gilbert, L.V. Slipchenko, S.V. Levchenko, D.P. O'Neill, R.A. DiStasio Jr., R.C. Lochan, T. Wang, G.J.O. Beran, N.A. Besley, J.M. Herbert, Y.C. Lin, T. Van Voorhis, S.H. Chien, A. Sodt, R.P. Steele, V.A. Rassolov, P.E. Maslen, P.P. Korambath, R.D. Adamson, B. Austin, J. Baker, E.F.C. Byrd, H. Dachsel, R.J. Doerksen, A. Dreuw, B.D. Dunietz, A.D. Dutoi, T.R. Furlani, S.R. Gwaltney, A. Heyden, S. Hirata, C.P. Hsu, G. Kedziora, R.Z. Khalliulin, P. Klunzinger, A.M. Lee, M.S. Lee, W.Z. Liang, I. Lotan, N. Nair, B. Peters, E.I. Proynov, P.A. Pieniazek, Y.M. Rhee, J. Ritchie, E. Rosta, C.D. Sherrill, A.C. Simmonett, J.E. Subotnik, H.L. Woodcock III, W.M. Zhang, A.T. Bell, A.K. Chakraborty, D.M. Chipman, F.J. Keil, A. Warshel, W.J. Hehre, H.F. Schaefer III, J. Kong, A.I. Krylov, P.M.W. Gill, M. Head-Gordon, Phys. Chem. Chem. Phys. 8 (2006) 3172.
[131] P. Sherwood, A.H. de Vries, M.F. Guest, G. Schreckenbach, C.R.A. Catlow, S.A. French, A.A. Sokol, S.T. Bromley, W. Thiel, A.J. Turner, S. Billeter, F. Terstegen, S. Thiel, J. Kendrick, S.C. Rogers, J. Casci, M. Watson, F. King, E. Karlsen, M. Sjøvoll, A. Fahmi, A. Schäfer, C. Lennartz, J. Mol. Struct.: THEOCHEM 632 (2003) 1.
[132] S.R. Billeter, A.J. Turner, W. Thiel, Phys. Chem. Chem. Phys. 2 (2000) 2177.
[133] W. Smith, T.R. Forester, J. Mol. Graphics 14 (1996) 136.
[134] J. Wang, R.M. Wolf, J.W. Caldwell, P.A. Kollman, D.A. Case, J. Comput. Chem. 25 (2004) 1157.
[135] D. Bakowies, W. Thiel, J. Phys. Chem. 100 (1996) 10580.
[136] W.R. Lambert, P.M. Felker, A.H. Zewail, J. Chem. Phys. 75 (1981) 5958.
[137] P. Irkhin, A. Ryasnyanskiy, M. Koehler, I. Biaggio, Phys. Rev. B 86 (2012) 85143.
[138] M. Banasiewicz, I. Deperasińska, B. Kozankiewicz, J. Phys. Chem. A 107 (2003) 662.
[139] M. Dierksen, S. Grimme, J. Chem. Phys. 120 (2004) 3544.
[140] J. Ferguson, L.W. Reeves, W.G. Schneider, Can. J. Chem. 35 (1957) 1117.
[141] T. Petrenko, O. Krylova, F. Neese, M. Sokolowski, New J. Phys. 11 (2009) 015001.
[142] F. Santoro, A. Lami, R. Improta, J. Bloino, V. Barone, J. Chem. Phys. 128 (2008) 224311.
[143] L. Edwards, D.H. Dolphin, M. Gouterman, A.D. Adler, J. Mol. Spectrosc. 38 (1971) 16.
[144] L. Edwards, D.H. Dolphin, J. Mol. Spectrosc. 35 (1970) 90.
[145] J. Šeda, J.V. Burda, J. Leszczynski, J. Comput. Chem. 26 (2005) 294.
[146] S. Lamansky, P. Djurovich, D. Murphy, F. Abdel-Razzaq, H. Lee, C. Adachi, P.E. Burrows, S.R. Forrest, M.E. Thompson, J. Am. Chem. Soc. 123 (2001) 4304.
[147] J. Li, P.I. Djurovich, B.D. Alleyne, I. Tsyba, N.N. Ho, R. Bau, M.E. Thompson, Polyhedron 23 (2004) 419.
[148] A.B. Tamayo, B.D. Alleyne, P.I. Djurovich, S. Lamansky, I. Tsyba, N.N. Ho, R. Bau, M.E. Thompson, J. Am. Chem. Soc. 125 (2003) 7377.
[149] T. Sajoto, P.I. Djurovich, A. Tamayo, M. Yousufuddin, R. Bau, M.E. Thompson, R.J. Holmes, S.R. Forrest, Inorg. Chem. 44 (2005) 7992.
[150] Y.Q. Jiang, Q. Peng, X. Gao, Z.G. Shuai, Y.L. Niu, S.H. Lin, J. Mater. Chem. 22 (2012) 4491.
[151] M. Wan, W. Wu, G. Sang, Y. Zou, Y. Liu, Y. Li, J. Polym. Sci. Part A: Polym. Chem. 47 (2009) 4028.
[152] M. Horie, I.W. Shen, S.M. Tuladhar, H. Leventis, S.A. Haque, J. Nelson, B.R. Saunders, M.L. Turner, Polymer 51 (2010) 1541.
[153] B. Lim, K. Baeg, H. Jeong, J. Jo, H. Kim, J. Park, Y. Noh, D. Vak, J. Park, J. Park, D. Kim, Adv. Mater. 21 (2009) 2808.
[154] L. Huo, T.L. Chen, Y. Zhou, J. Hou, H. Chen, Y. Yang, Y. Li, Macromolecules 42 (2009) 4377.
[155] J. Luo, Z. Xie, J.W.Y. Lam, L. Cheng, H. Chen, C. Qiu, H.S. Kwok, X. Zhan, Y. Liu, D. Zhu, B.Z. Tang, Chem. Commun. (2001) 1740.
[156] Y. Hong, J.W.Y. Lam, B.Z. Tang, Chem. Commun. (2009) 4332.
[157] J. Liu, J.W.Y. Lam, B.Z. Tang, J. Inorg. Organomet. Polym. Mater. 19 (2009) 249.
[158] M. Wang, G. Zhang, D. Zhang, D. Zhu, B.Z. Tang, J. Mater. Chem 20 (2010) 1858.
[159] D. Ding, K. Li, B. Liu, B.Z. Tang, Acc. Chem. Res. 46 (2013) 2441.
[160] J. Chen, C.C.W. Law, J.W.Y. Lam, Y. Dong, S.M.F. Lo, I.D. Williams, D. Zhu, B.Z. Tang, Chem. Mater. 15 (2003) 1535.
[161] Z. Li, Y. Dong, B. Mi, Y. Tang, M. Häussler, H. Tong, Y. Dong, J.W.Y. Lam, Y. Ren, H.H.Y. Sung, K.S. Wong, P. Gao, I.D. Williams, H.S. Kwok, B.Z. Tang, J. Phys. Chem. B 109 (2005) 10061.
[162] B. An, D. Lee, J. Lee, Y. Park, H. Song, S.Y. Park, J. Am. Chem. Soc. 126 (2004) 10232.
[163] B. An, S. Kwon, S. Jung, S.Y. Park, J. Am. Chem. Soc. 124 (2002) 14410.
[164] Y. Liu, X. Tao, F. Wang, J. Shi, J. Sun, W. Yu, Y. Ren, D. Zou, M. Jiang, J. Phys. Chem. C 111 (2007) 6544.
[165] Y. Sonoda, S. Tsuzuki, M. Goto, N. Tohnai, M. Yoshida, J. Phys. Chem. A 114 (2009) 172.
[166] R. Hu, E. Lager, A. Aguilar-Aguilar, J. Liu, J.W.Y. Lam, H.H.Y. Sung, I.D. Williams, Y. Zhong, K.S. Wong, E. Peña-Cabrera, B.Z. Tang, J. Phys. Chem. C 113 (2009) 15845.
[167] S. Xiao, Y. Zou, J. Wu, Y. Zhou, T. Yi, F. Li, C. Huang, J. Mater. Chem. 17 (2007) 2483.
[168] Q. Peng, Y.P. Yi, Z.G. Shuai, J.S. Shao, J. Am. Chem. Soc. 129 (2007) 9333.
[169] Q. Peng, Y.L. Niu, C.M. Deng, Z.G. Shuai, Chem. Phys. 370 (2010) 215.
[170] C.M. Deng, Y.L. Niu, Q. Peng, A.J. Qin, Z.G. Shuai, B.Z. Tang, J. Chem. Phys. 135 (2011) 014304.
[171] Q.Y. Wu, Q. Peng, Y.L. Niu, X. Gao, Z.G. Shuai, J. Phys. Chem. A 116 (2012) 3881.
[172] Q. Peng, Y.L. Niu, Z.H. Wang, Y. Jiang, Y. Li, Y. Liu, Z.G. Shuai, J. Chem. Phys. 134 (2011) 074510.
[173] S.K. Chattopadhyay, P.K. Das, G.L. Hug, J. Am. Chem. Soc. 104 (1982) 4507.
[174] W.A. Yee, S.J. Hug, D.S. Kliger, J. Am. Chem. Soc. 110 (1988) 2164.
[175] N.I. Nijegorodov, W.S. Downey, J. Phys. Chem. 98 (1994) 5639.
[176] I. Deperasińska, B. Kozankiewicz, I. Biktchantaev, J. Sepioł, J. Phys. Chem. A. 105 (2001) 810.
[177] A. Asefa, A.K. Singh, J. Lumin. 130 (2010) 24.
[178] A. Qin, J.W.Y. Lam, F. Mahtab, C.K.W. Jim, L. Tang, J. Sun, H.H.Y. Sung, I.D. Williams, B.Z. Tang, Appl. Phys. Lett. 94 (2009) 253308.
[179] H. Tong, Y. Dong, M. Häussler, J.W.Y. Lam, H.H.Y. Sung, I.D. Williams, J. Sun, B.Z. Tang, Chem. Commun. (2006) 1133.
[180] K. Dahl, R. Biswas, M. Maroncelli, J. Phys. Chem. B 107 (2003) 7838.
[181] W.A. Yee, J.S. Horwitz, R.A. Goldbeck, C.M. Einterz, D.S. Kliger, J. Phys. Chem. 87 (1983) 380.
[182] E. Clar, Polycyclic Hydrocarbons, vol. 2, Academic, London, 1964.
[183] J.B. Birks, Photophysics of Atomic Molecules, Wiley, London, 1973.
[184] M. Sonnenschein, A. Amirav, J. Jortner, J. Phys. Chem. 88 (1984) 4214.
[185] J. Chen, B. Xu, X. Ouyang, B.Z. Tang, Y. Cao, J. Phys. Chem. A 108 (2004) 7522.
[186] G. Yu, S. Yin, Y. Liu, J. Chen, X. Xu, X. Sun, D. Ma, X. Zhan, Q. Peng, Z. Shuai, B. Tang, D. Zhu, W. Fang, Y. Luo, J. Am. Chem. Soc. 127 (2005) 6335.
[187] Z.G. Shuai, W.J. Liu, W.Z. Liang, Q. Shi, H. Chen, Sci. Chin. Chem. 56 (2013) 1258.
[188] T. Yanai, Y. Kurashige, E. Neuscamman, G.K.L. Chan, J. Chem. Phys. 132 (2010) 024105.
[189] S. Baroni, S. de Gironcoli, A. Dal Corso, P. Giannozzi, Rev. Modern Phys. 73 (2001) 515.